Learning to Foresee: Unveiling the Unlocking Efficiency of On-Policy Distillation

Yuchen Cai[1,2†], **Ding Cao**[1,4*], **Liang Lin**[5], **Chunxi Luo**[6], **Xin Xu**[2], **Kai Yang**[2], **Weijie Liu**[2], **Saiyong Yang**[2], **Tianxiang Zhao**[4], **Guangzhong Sun**[1], **Guiquan Liu**[1‡], **Junfeng Fang**[3‡]

[1]USTC, [2]Tencent, [3]NUS, [4]HKUST(GZ), [5]UCAS-IIE, [6]SHU

{caiyuchen,caoding}@mail.ustc.edu.cn

Abstract

On-policy distillation (OPD) has emerged as an efficient post-training paradigm for large language models. However, existing studies largely attribute this advantage to denser and more stable supervision, while the parameter-level mechanisms underlying OPD's efficiency remain poorly understood. In this work, we argue that OPD's efficiency stems from a form of "foresight": it establishes a stable update trajectory toward the final model early in training. This foresight manifests in two aspects. First, at the **Module-Allocation Level**, OPD identifies regions with low marginal utility and concentrates updates on modules that are more critical to reasoning. Second, at the **Update-Direction Level**, OPD exhibits stronger low-rank concentration, with its dominant subspaces aligning closely with the final update subspace early in training. Building on these findings, we propose **EffOPD**, a plug-and-play acceleration method that speeds up OPD by adaptively selecting an extrapolation step size and moving along the current update direction. EffOPD requires no additional trainable modules or complex hyperparameter tuning, and achieves an average training acceleration of 3× while maintaining comparable final performance. Overall, our findings provide a parameter-dynamics perspective for understanding the efficiency of OPD and offer practical insights for designing more efficient post-training methods for large language models. Our code is available at: https://github.com/caiyuchen-ustc/EffOPD.

"To foresee the future is to master the present."
— Niccolò Machiavelli

1 Introduction

As large language models (LLMs) continue to advance in reasoning (OpenAI, 2025; DeepSeek-AI et al., 2025), On-Policy Distillation (OPD) has emerged as an important paradigm for post-training and model fusion (Agarwal et al., 2024b; Xiao et al., 2026; DeepSeek-AI, 2026). Given a teacher model, OPD leverages dense supervisory signals to achieve performance comparable to Reinforcement Learning (RL) with substantially reduced training time (Venkatkrishna et al., 2026; Yang et al., 2025). Existing studies mainly attribute this advantage to denser and more stable supervision (He et al., 2026; Yue et al., 2025). However, such optimization-centric explanations remain largely macroscopic and fail to capture the underlying parameter update dynamics (Zhang et al., 2025b).

*These authors contributed equally to this work.
†This work was done during an internship at Tencent.
‡Corresponding authors: gqliu@ustc.edu.cn, fjf@mail.ustc.edu.cn

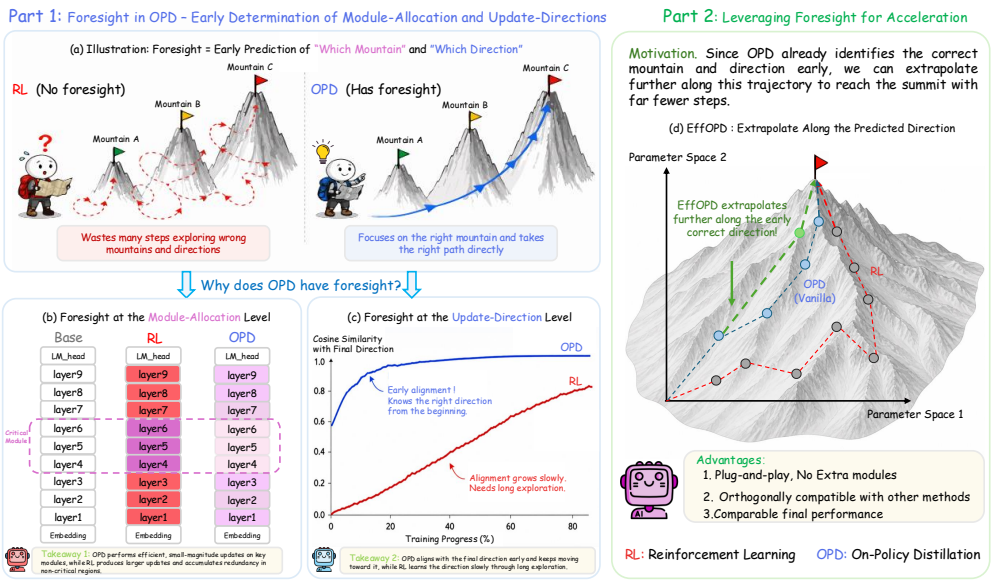

Figure 1: Illustration of the foresight mechanism in OPD. Compared with RL, OPD identifies critical modules and aligns with the final optimization direction early in training, concentrating effective updates while reducing redundancy. Based on this, we propose EffOPD, which extrapolates along the early predicted direction to accelerate training.

In this work, we argue that OPD's efficiency stems from a form of "foresight": it establishes stable and highly aligned update directions early in training, enabling rapid convergence with limited exploration and correction. This foresight manifests in two aspects.

Foresight at the Module-Allocation Level. Our analysis reveals that, under the same update norm constraint, OPD achieves larger performance gains than RL, suggesting that its advantage does not merely stem from the magnitude of parameter updates (Geva et al., 2021, 2023). Further analysis shows that, although RL and OPD exhibit similar sensitivity patterns across layers and modules, RL accumulates substantially larger update norms in modules with limited contribution to performance improvement, thereby introducing redundant updates with low marginal utility. In contrast, OPD demonstrates a form of "foresight". As shown in Figure 1 (b), it identifies these low-utility modules early in training and suppresses their parameter updates, allowing updates to concentrate more effectively on intermediate-layer modules that are more critical to reasoning (Meng et al., 2023).

Foresight at the Update-Direction Level. At the update-direction level, OPD's foresight lies in the early alignment between its update directions and the principal directions of the final solution. Spectral and subspace evolution analyses show that OPD concentrates updates on a few stable dominant directions early in training (Zhang, 2015), whose dominant directions are highly aligned with the final update subspace and remain stable thereafter, as shown in Figure 1 (c). In contrast, RL exhibits more dispersed updates, with delayed and more fluctuating alignment. Moreover, after module-wise norm scaling, an OPD checkpoint at only 10% training progress recovers approximately 80% of the final reasoning performance. This suggests that OPD captures the main structure of the final solution early and locks onto an effective direction with minimal exploration and correction.

To further validate these insights and improve the training efficiency of OPD, we propose **EffOPD**, a simple and intuitive acceleration framework. As shown in Figure 1 (d), EffOPD performs linear extrapolation along the current update direction, leveraging the inherent "foresight" of OPD to match the final performance of vanilla OPD with fewer training iterations and samples. Experiments across model scales from 1.5B to 32B parameters show that EffOPD achieves an average training acceleration of $3\times$ over multiple baselines in a plug-and-play manner, while maintaining comparable final performance.

In summary, this work identifies a form of foresight in OPD for LLMs and argues that it is a key source of its training efficiency. Our analysis provides a parameter-level explanation for the common intuition that distillation is easier to optimize due to denser supervision (Yang et al., 2026a). Building

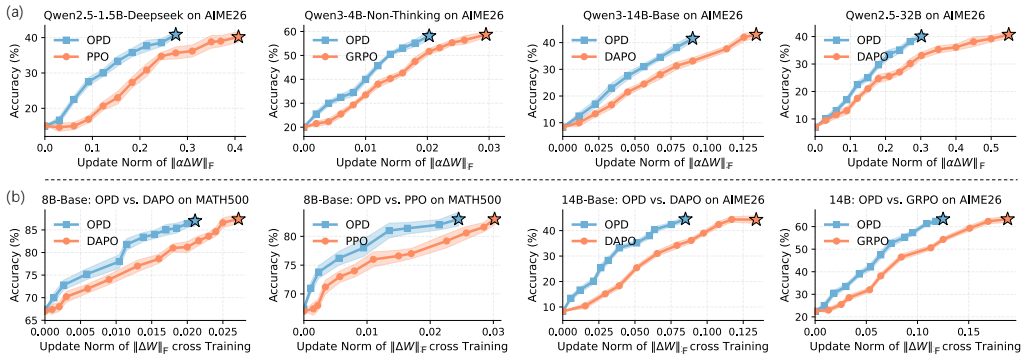

Figure 2: Comparison of parameter update efficiency between RL and OPD. (a) Scaling analysis at the final checkpoint: for updates scaled to the same norm, OPD achieves substantially higher reasoning gains than RL. (b) Training dynamics: across the entire optimization trajectory, OPD consistently requires smaller parameter updates than RL to reach equivalent reasoning accuracy.

on these findings, EffOPD offers a simple plug-and-play acceleration method for OPD, requiring no additional modules, complex hyperparameter tuning, or human intervention. It achieves an average training acceleration of $3\times$ and remains orthogonal to existing acceleration techniques, providing new insights into the design of more interpretable and efficient post-training paradigms for large language models.

2 Functional Redundancy Avoidance

In this section, we investigate the modular-level differences between OPD and RL. We show that OPD exhibits modular-level "foresight": it preferentially concentrates updates in high-marginal-utility functional regions while suppressing parameter changes in low-utility regions. We refer to this property as **Functional Redundancy Avoidance**. Section 2.1 introduces the experimental setup, and Section 2.2 compares OPD with RL to show how this foresight leads to more compact and efficient parameter updates.

2.1 Experimental Setting

Our analysis uses a shared initialization W_{Base} for both RL and OPD, with parameter updates defined as $\Delta W_{\text{RL/OPD}} = W_{\text{RL/OPD}} - W_{\text{Base}}$. We conduct experiments across models ranging from 1.5B to 32B parameters, including pretrained, SFT-tuned, and Thinking-series models (Qwen et al., 2025; Zhang et al., 2025c; Yang et al., 2025). For RL, we consider PPO, GRPO, and DAPO (Yu et al., 2025). For OPD, the student is trained with a pattern-aligned teacher, typically a stronger model from the same family (Li et al., 2026). Further details are provided in Appendix D.2.

2.2 Parameter Updates & Reasoning Gains

Results on Fully Trained Models. We first examine the update efficiency at the final checkpoint. Specifically, we fix the update direction $\Delta W_{\text{RL/OPD}}$ from the last checkpoint and scale its magnitude using a factor $\alpha \in [0, 1]$, evaluating models of the form $W_{\text{Base}} + \alpha \Delta W_{\text{RL/OPD}}$. As shown in Figure 2 (a), when updates are scaled to the same norm, OPD achieves substantially higher reasoning gains than RL. This indicates that ΔW_{RL} contains a non-negligible number of components weakly correlated with task performance—they contribute to the update norm but provide limited reasoning improvement. In contrast, OPD updates carry a greater fraction of task-relevant signal that effectively translates into performance gains.

Results across the Training Process. This observation naturally raises a key question: when do these weakly task-correlated components emerge during RL training? Since the performance of RL-trained models typically saturates in later stages, one possible explanation is that redundant updates mainly accumulate near the end of training (Khatri et al., 2025; Zheng et al., 2025). To

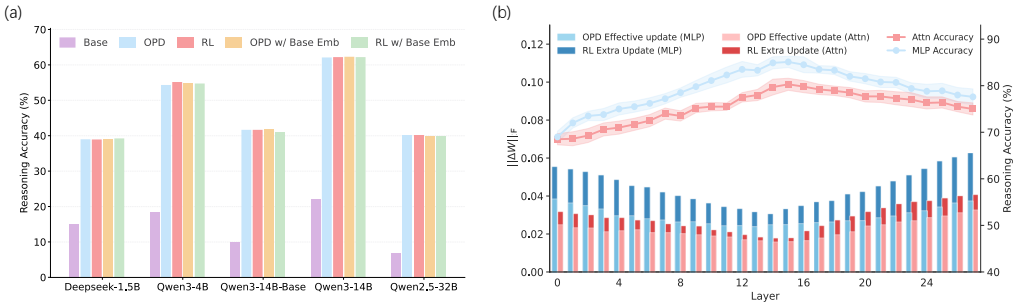

Figure 3: Functional contributions and update distributions across architectural components. (a) Effect of embedding layer replacement on AIME26. (b) Layer-wise update norms (bars, left axis) for RL/OPD-trained Qwen3-8B-Base models, and corresponding OPD reasoning accuracy after sliding-window intervention (line, right axis) on MATH500.

examine this, we analyze intermediate checkpoints of both RL and OPD throughout training and track the relationship between parameter update magnitude and reasoning accuracy. As shown in Figure 2 (b), OPD consistently requires smaller parameter updates than RL to achieve the same reasoning accuracy. Moreover, OPD achieves rapid accuracy improvement with relatively small increases in ΔW_{OPD} norm, whereas RL improves more slowly under comparable update magnitudes. These results suggest that OPD's superior efficiency does not simply come from avoiding late-stage redundancy, but from forming a compact and task-relevant update pattern early in training.

Locating the Redundant Updates. The previous analysis shows that RL updates contain components with relatively low task relevance. To locate these redundancies and assess their functional contributions, we decompose model updates into three architectural components: embedding, MLP, and attention layers. We first examine the embedding layer by replacing the embeddings of OPD and RL models with those from the base model while keeping all other parameters unchanged. As shown in Figure 3 (a), this intervention has negligible impact on reasoning performance, suggesting that embedding updates contribute little to reasoning gains. Thus, the main functional updates of OPD and RL are likely concentrated in deeper model components rather than the embedding layer.

Next, we conduct a sliding-window intervention analysis to locate the functional regions of OPD and RL updates. Following prior block-wise intervention studies (Cai et al., 2024; Meng et al., 2023), we partition the model into consecutive layer blocks and inject local OPD or RL updates into each block to evaluate their impact on reasoning performance[4]. As shown in Figure 3 (b) and Figure 10 (b), MLP modules are overall more sensitive to reasoning-related updates than attention modules, indicating that MLPs serve as the primary carriers of knowledge representation and relational reasoning. From the perspective of layer position, the performance curves of both module types exhibit a clear inverted U-shaped pattern: interventions in the middle layers yield the largest gains, whereas those in the bottom and top layers lead to relatively smaller improvements. This suggests that reasoning-related updates are not uniformly distributed across the network, but are mainly concentrated in middle-layer MLPs with stronger functional coupling. These findings are consistent with prior mechanistic interpretability studies on the functional roles of Transformer modules and layers (Skean et al., 2025; Geva et al., 2021, 2022).

Building on these observations, we further compare the update patterns of OPD and RL. The two methods exhibit highly consistent intervention sensitivity distributions across both module types and layer positions, suggesting that OPD and RL do not rely on fundamentally different functional pathways, but instead optimize along the model's existing key functional structures. The key difference lies in their layer-wise update norms. RL introduces substantially larger parameter changes in the low-sensitivity bottom and top layers. Since interventions in these peripheral layers yield limited performance gains, their larger update norms do not translate into proportional performance gains and are therefore more likely to reflect redundant updates weakly related to task rewards. In contrast, while maintaining a functional update distribution similar to RL, OPD significantly suppresses parameter changes in low-sensitivity regions and concentrates updates more strongly in

[4]Detailed setup is provided in Appendix E.2.

Table 1: Characterization of Parameter Update Geometry: OPD vs. RL Across Model Scales.

Metric	1.5B		4B		8B		14B	
	RL	OPD	RL	OPD	RL	OPD	RL	OPD
Spectral Norm (↑)	0.094	0.113	0.007	0.009	0.004	0.005	0.056	0.063
Spectral / Frobenius Norm Ratio (↑)	33.2%	39.6%	19.7%	25.7%	32.7%	36.8%	24.4%	28.1%
Effective Rank (↓)	964	778	1908	1587	2754	2341	3174	2937
Top-1% Subspace Norm Ratio (↑)	78.1%	92.3%	79.2%	93.4%	88.5%	94.7%	81.2%	94.5%

middle-layer modules with higher functional contributions. Therefore, the advantage of OPD does not come from learning an entirely new update mechanism, but from more accurately distinguishing high-benefit from low-benefit parameter regions and reducing ineffective updates in peripheral layers, thereby achieving higher update efficiency and stronger reasoning performance gains with more compact parameter changes. Additionally, we further present the visualized differences and performance comparison results between RL and OPD across different components. We recommend interested readers to refer to the detailed results and analysis in Appendix E.

Summary. The above results show that OPD exhibits clear foresight at the modular level, which we formalize as Property 1: **Functional Redundancy Avoidance**. Compared with RL, OPD forms a compact and task-relevant update pattern earlier in training, suppresses redundant parameter changes in low-marginal-utility regions, and concentrates updates in reasoning-critical modules with higher functional contributions, thereby achieving higher update efficiency and stronger reasoning performance gains.

3 Early Low-Rank Lock-in

The preceding analysis reveals OPD's "foresight" at the modular level. Building on this, we further investigate the intrinsic organization of its parameter updates from a geometric perspective and introduce the property **Early Low-Rank Lock-in** to describe this potential structural constraint. Specifically, we validate this property by analyzing the spectral concentration of the update matrix, the functional contributions of different subspaces, and the functional effectiveness of early stabilized directions through norm scaling experiments.

3.1 Spectral Concentration of Update Matrix

To characterize the spectral structure of parameter updates, we perform singular value decomposition (SVD) (Koren et al., 2009) on the update matrix $\Delta W_{\mathrm{RL/OPD}} = U\Sigma V^\top$ and introduce four complementary geometric metrics[5]: **Spectral Norm** (Mathias, 1990), **Spectral / Frobenius Norm Ratio** (Al-Natoor, 2024), **Effective Rank** (Roy & Vetterli, 2007), and **Top-1% Subspace Norm Ratio** (Cai et al., 2025). The first two metrics quantify the dominance of leading singular directions, while the latter two measure the concentration of update energy across the spectrum. Table 1 reports the average values over all MLP and attention matrices. Across all model scales, OPD consistently exhibits stronger low-rank structure than RL. For example, on the 8B model, OPD achieves a higher spectral-to-Frobenius norm ratio (36.8% vs. 32.7%), lower effective rank (2341 vs. 2754), and higher Top-1% subspace norm ratio (94.7% vs. 88.5%). These results suggest that OPD concentrates update energy into a small set of dominant directions more effectively than RL. Notably, despite having a smaller overall update norm, OPD allocates a larger proportion of its update energy to these dominant subspaces. This raises a key question: does such directional concentration explain the efficiency advantage of OPD observed in Section 2? To answer this, we conduct two controlled experiments to separately examine the roles of update direction and update magnitude.

3.2 Functional Partition of the Update Spectrum: Principal vs. Tail Subspaces

Top-$k\%$ Subspace: Directional Quality under Equal Norm Budget. To assess the intrinsic directional quality of the principal subspace, we construct a Top-$k\%$ truncated approximation $\Delta W_{\text{Top-}k\%}$

[5]Detailed definitions are provided in Appendix F.1.

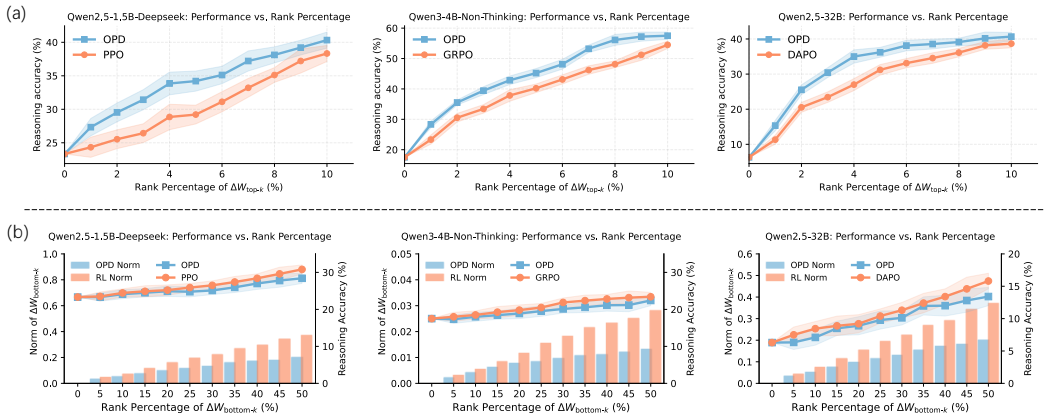

Figure 4: Low-rank subspace analysis. (a) Top-$k\%$ subspace: OPD achieves higher performance; (b) Bottom-$k\%$ subspace: RL incurs significantly larger norm cost for marginal performance gains.

using the Top-$k\%$ singular components, and subsequently rescale its Frobenius norm to match between RL and OPD. After applying this low-rank update to the base model, we evaluate its reasoning performance. By standardizing the norm budget, we are able to directly compare the directional quality of the Top-$k\%$ principal subspaces between RL and OPD.

As shown in Figure 4 (a), both methods recover over 95% of their full-model reasoning performance using only 10% of the rank, confirming that the Top-$k\%$ subspace serves as the primary carrier for improving reasoning performance. Remarkably, OPD consistently outperforms RL across all evaluated rank levels, and this advantage persists across different model scales and rank thresholds. This suggests not only that OPD allocates its limited update budget more efficiently by concentrating on higher-quality directional subspaces, but also that the principal directions identified by OPD inherently encode more effective update signals than those of RL, even under the same norm budget.

Bottom-$k\%$ Subspace: Marginal Utility of Tail Directions. To further investigate, we compare the impact of tail directions on performance, where tail directions are defined as the subspace constructed using the last $k\%$ singular components, denoted as $\Delta W_{\text{Bottom-}k\%}$. Unlike the Top-$k\%$ subspace analysis, we do not apply norm scaling to equalize the update budgets, so as to observe their performance contributions under the original training state. As shown in Figure 5 (b), in contrast to the principal subspace, tail subspaces provide only limited performance recovery for both RL and OPD. On the Qwen2.5-1.5B-DeepSeek model, retaining only 10% of the principal subspace increases reasoning accuracy from 23.33% to 40.3%, whereas preserving 50% of the tail subspace achieves only around 30%, despite using a much larger fraction of the rank budget. This contrast suggests that tail directions have substantially lower marginal utility for reasoning than principal directions.

Interestingly, RL exhibits a slight advantage over OPD in tail directions. However, this marginal benefit comes with a large norm cost: the norm of RL's tail subspace ($\Delta W_{\text{Bottom-}50\%}$) ranges from approximately 1.6 to 2.5 times that of OPD, while the corresponding performance gain remains limited. In other words, RL allocates a substantial portion of its update magnitude to tail directions, but the marginal return of this allocation is relatively low.

These observations help explain the compactness advantage of OPD discussed in Section 2. Compared with OPD, RL distributes more update energy into tail directions whose contribution to reasoning performance is limited, which is consistent with its larger overall update norm for comparable performance. In contrast, OPD allocates a larger fraction of its update energy to the principal subspace, thereby achieving stronger per-norm performance gains with more compact updates.

The preceding analysis shows that OPD updates exhibit substantially stronger low-rank concentration from a spatial-geometric perspective. Together with the controlled Top-$k\%$ and Bottom-$k\%$ subspace experiments, this suggests that such concentration is a key factor behind OPD's higher per-norm efficiency, rather than merely a by-product of smaller update norms. We next move from static spectral structure to temporal evolution, examining whether OPD's efficiency arises from early identification of high-quality directions or from continuous path correction during training.

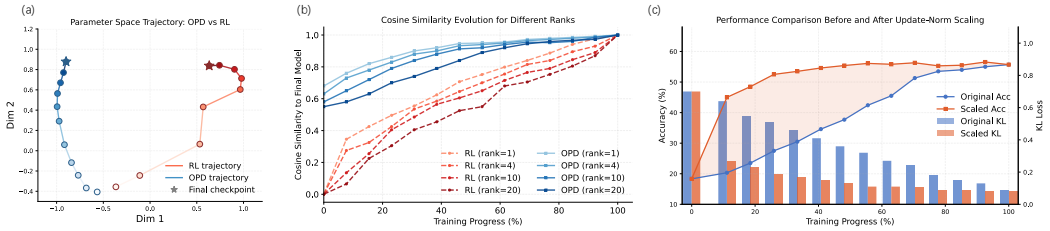

Figure 5: Subspace evolution and weight scaling analysis during training. (a) t-SNE visualization of Top-1 subspace evolution for RL and OPD trajectories. (b) Cosine similarity between the Top-k subspaces of intermediate and final checkpoints. (c) Changes in Accuracy and KL after scaling intermediate OPD checkpoints' ΔW_{OPD} to match the final checkpoint's norm.

3.3 Directional Stabilization and Magnitude Development

Subspace Evolution Trajectory Analysis. To qualitatively compare the evolution of update directions during training, we visualize the Top-1 subspace using t-SNE, as shown in Figure 5 (a). The RL trajectory exhibits larger variations across checkpoints, whereas the OPD trajectory appears more compact and smoother in the projected space. This visualization suggests a potential difference in directional stability between RL and OPD, which we next examine quantitatively through subspace alignment analysis.

Specifically, we pair each Top-k subspace ($k = 1, \ldots, 20$) from each training step with its corresponding subspace in the final checkpoint, compute the cosine similarity, and then average over k. The results are shown in Figure 5 (b). OPD consistently exhibits stronger alignment with its final subspaces than RL across all evaluated ranks, with smaller fluctuations throughout training. This difference is particularly pronounced in the early stage of training (0%–30%), indicating that OPD stabilizes its dominant update directions earlier than RL, and that this stability extends beyond the Rank-1 direction to multiple dominant subspaces.

Magnitude Scaling and Performance Recovery. The preceding subspace-alignment analysis shows that the dominant OPD update subspaces are already strongly aligned with their final counterparts at an early stage of training. Based on this observation, we further investigate the source of the remaining performance gap in early checkpoints: whether this gap arises from insufficiently formed effective update directions, or from underdeveloped update magnitudes along these directions.

To examine this hypothesis, we perform a module-wise norm-scaling intervention on intermediate OPD checkpoints. For each intermediate checkpoint, we preserve the update direction within each module, while rescaling its Frobenius norm to match that of the corresponding module in the final checkpoint. We then apply the rescaled update to the base model and evaluate the resulting model, as shown in Figure 5 (c). This intervention allows us to assess how much performance can be recovered when early update directions are given the same module-wise norm budget as the final checkpoint.

The results show that norm scaling markedly improves the performance of early checkpoints. In particular, a checkpoint at only 10% training progress recovers approximately 80% of the final model's performance after scaling. We also observe a reduction in the KL divergence between the rescaled checkpoints and the teacher model, indicating that the scaled updates move the student output distribution closer to the teacher distribution. These results suggest that early OPD checkpoints already possess task-relevant update directions, while the limited update magnitudes become a bottleneck that constrains further performance improvement.

Overall, these experiments separate two aspects of the OPD update trajectory, namely the formation of dominant directions and the growth of update magnitudes, thereby complementing the subspace alignment analysis. Experimental evidence shows that OPD establishes stable update directions early in training, with subsequent training primarily accumulating magnitude along these directions rather than making large-scale adjustments to the directions themselves. We further analyze the geometric and theoretical manifestations of Property 2 in Appendix F.2-F.5.

Summary. This section reveals the core geometric characteristics of OPD's parameter updates. OPD's updates exhibit stronger low-rank concentration and stabilize their dominant subspaces early,

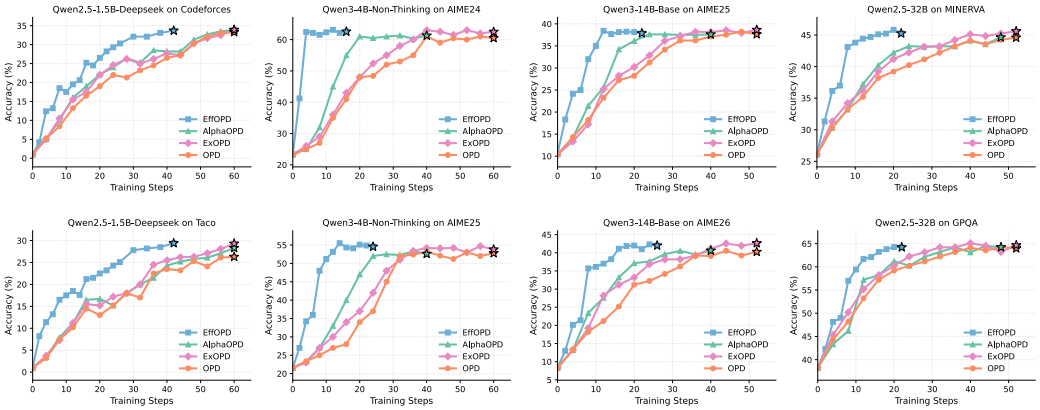

Figure 6: Performance comparison of different distillation methods on code and math datasets.

with subsequent training mainly progressing along these subspaces. We term this **Property 2: Early Low-Rank Lock-in**, which structurally explains **Property 1: Functional Redundancy Avoidance**. By locking into efficient low-rank directions early, OPD reduces reliance on redundant exploration and correction, avoids overlearning redundant information, and exhibits stronger foresight at the modular level.

4 Accelerating OPD via Directional Extrapolation

The preceding analysis suggests that OPD establishes highly stable and final-aligned update directions early in training. After this early directional lock-in, later optimization mainly amplifies the update magnitude along the same trajectory, rather than exploring new directions. Motivated by this observation, we propose **EffOPD**, a plug-and-play acceleration framework that exploits early directional extrapolation to accelerate OPD. We next detail the acceleration procedure and report the corresponding empirical results.

4.1 Method

Let W_t denote the model parameters after the t-th OPD update. EffOPD triggers an extrapolation search at exponentially spaced checkpoints, i.e., when $t = 2^n$ with n starting from 0, so the first extrapolation is performed at $t = 1$. For the first checkpoint, we use the displacement from the initial parameters to W_1 as the local update direction. For subsequent checkpoints with $n \geq 1$, EffOPD estimates the local update direction using the parameter displacement between the current exponential checkpoint and the previous one:

$$\Delta_n = W_{2^n} - W_{2^{n-1}}. \tag{1}$$

This displacement captures the accumulated parameter evolution between two adjacent exponential checkpoints. Since OPD update directions remain relatively stable during training, Δ_n serves as a local approximation of subsequent update directions.

EffOPD then generates five candidate parameters from W_{2^n} along Δ_n with increasing extrapolation magnitudes. For $k = 1, 2, \cdots, 5$, the k-th candidate is defined as:

$$\widetilde{W}_{n,k} = W_{2^n} + 2k\Delta_n, \tag{2}$$

where the coefficient $2k$ controls the extrapolation scale. To determine whether the extrapolated parameters remain effective, EffOPD randomly samples 50 examples from the training set to form a lightweight validation set $\mathcal{D}_v$, which is far smaller than the number of sentences generated per step in vanilla OPD. sLet $\mathcal{V}_{\mathcal{D}_v}(\cdot)$ denote the validation function. EffOPD initializes the accepted parameters as $W^{\text{acc}} = W_{2^n}$ and its score as $v^{\text{acc}} = \mathcal{V}_{\mathcal{D}_v}(W_{2^n})$. Then EffOPD evaluates $\widetilde{W}_{n,k}$ sequentially. If $\mathcal{V}_{\mathcal{D}_v}(\widetilde{W}_{n,k}) \geq v^{\text{acc}}$, the candidate is accepted, and we update:

$$W^{\text{acc}} \leftarrow \widetilde{W}_{n,k}, \quad v^{\text{acc}} \leftarrow \mathcal{V}_{\mathcal{D}_v}(\widetilde{W}_{n,k}). \tag{3}$$

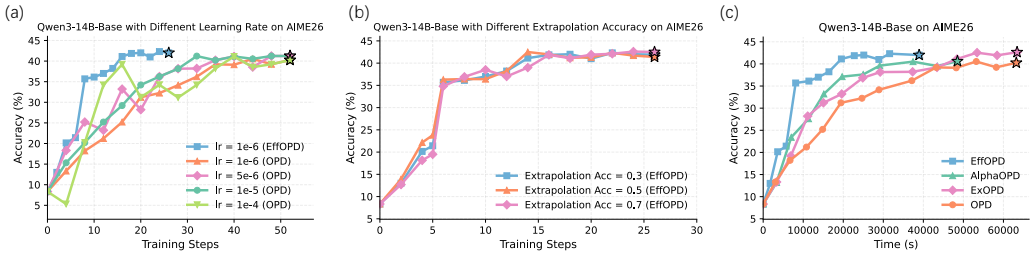

Figure 7: Ablation studies. (a) Effect of different learning rates. (b) Impact of $\mathcal{D}_v$ difficulty on EffOPD. "Extrapolation Acc" denotes the accuracy of the model before training on the sampled $\mathcal{D}_v$. (c) Relationship between training time and performance.

If the current candidate fails to improve validation performance, the search terminates immediately. Thus, the final accepted parameters $W_{2^n}^{\mathrm{EffOPD}}$ at checkpoint 2^n is:

$$W_{2^n}^{\mathrm{EffOPD}} = W^{\mathrm{acc}}. \tag{4}$$

In particular, if the candidate with $k = 1$ already fails, EffOPD degenerates to vanilla OPD. This progressive extrapolation and immediate validation mechanism enables EffOPD to exploit the early directional stability of OPD while avoiding performance degradation caused by excessive extrapolation.

4.2 Main Results

To evaluate EffOPD, we conduct experiments on code generation and mathematical reasoning. We use Eurus-RL-Code (Cui et al., 2025a) and DeepMath-103K (Yang et al., 2026a) for training, and evaluate models at four scales: 1.5B, 4B, 14B, and 32B. For each scale, the RL-finetuned model serves as the teacher. We report results on seven benchmarks: Codeforces, Taco (Liu et al., 2023), AIME24, AIME25, AIME26, MINERVA, and GPQA (Ye et al., 2025). We compare EffOPD with Vanilla OPD, AlphaOPD (Cai et al., 2025), and ExOPD (Yang et al., 2026a).

As shown in Figure 6, EffOPD consistently improves training efficiency across all model scales and datasets. On mathematical reasoning tasks, it typically begins to converge within about 10 training steps, compared with 30–40 steps for vanilla OPD, yielding more than a $3\times$ speedup. EffOPD also reaches a higher performance upper bound, possibly because prolonged vanilla OPD training may cause over-optimization and semantic drift. Unlike AlphaOPD and ExOPD, which use fixed extrapolation strategies, EffOPD adaptively selects the extrapolation magnitude via validation feedback, leading to more stable acceleration. Its early-stage advantage is especially evident on Qwen3-4B-Non-Thinking, where EffOPD attains strong reasoning performance by the 4th step, further supporting that OPD forms high-quality, well-aligned update directions early in training.

Ablation Studies. We conduct ablation studies to identify the key factors behind EffOPD's effectiveness. As shown in Figure 7 (a), the learning rate strongly affects the stability of vanilla OPD: larger learning rates accelerate early convergence but also cause noticeable oscillations and performance instability. In contrast, EffOPD uses lightweight validation during extrapolation to adaptively filter out overly aggressive steps, thereby improving training stability. Figure 7 (b) shows that the difficulty of the lightweight validation set $\mathcal{D}_v$ is not critical. Validation sets of different difficulty levels provide consistent directional signals, suggesting that validation mainly serves to check whether the current update direction remains effective rather than to provide precise supervision. Figure 7 (c) compares actual training time. Despite the additional validation overhead, EffOPD achieves better performance under the same time budget and converges faster than vanilla OPD, indicating that the gain from exploiting early-stage update directions outweighs the validation cost. Overall, these results support the proposed foresight mechanism: once OPD establishes effective directions early in training, EffOPD can safely extrapolate along them to achieve stable and efficient acceleration.

5 Conclusion

In this work, we identify two properties that reveal the underlying "foresight" of OPD: **Functional Redundancy Avoidance** at the modular level and **Early Low-Rank Lock-in** at the update-direction

level. Through parameter-level analyses across model scales, RL algorithms, and task domains, we show that OPD achieves RL-comparable reasoning gains with more compact and structured updates, as it concentrates optimization on high-utility modules and directions from the early stage of training. Building on this insight, we propose **EffOPD**, a plug-and-play acceleration method that leverages early directional stability to achieve up to $3\times$ training speedup while maintaining the final performance. Overall, our findings suggest that OPD's efficiency is fundamentally tied to early directional stabilization and compact parameter allocation, offering a new perspective for understanding and accelerating post-training in large language models.

References

Rishabh Agarwal, Nino Vieillard, Yongchao Zhou, Piotr Stanczyk, Sabela Ramos Garea, Matthieu Geist, and Olivier Bachem. On-policy distillation of language models: Learning from self-generated mistakes. In *The twelfth international conference on learning representations*, 2024a.

Rishabh Agarwal, Nino Vieillard, Yongchao Zhou, Piotr Stanczyk, Sabela Ramos, Matthieu Geist, and Olivier Bachem. On-policy distillation of language models: Learning from self-generated mistakes, 2024b. URL https://arxiv.org/abs/2306.13649.

Ahmad Al-Natoor. Norm inequalities for functions of matrices. *Heliyon*, 10(9):e30056, 2024. ISSN 2405-8440. doi: https://doi.org/10.1016/j.heliyon.2024.e30056. URL https://www.sciencedirect.com/science/article/pii/S2405844024060870.

Yuchen Cai, Ding Cao, Rongxi Guo, Yaqin Wen, Guiquan Liu, and Enhong Chen. Locating and mitigating gender bias in large language models, 2024. URL https://arxiv.org/abs/2403.14409.

Yuchen Cai, Ding Cao, Xin Xu, Zijun Yao, Yuqing Huang, Zhenyu Tan, Benyi Zhang, Guangzhong Sun, Guiquan Liu, and Junfeng Fang. On predictability of reinforcement learning dynamics for large language models. *arXiv preprint arXiv:2510.00553*, 2025.

Zhipeng Chen, Tao Qian, Wayne Xin Zhao, and Ji-Rong Wen. Low-rank optimization trajectories modeling for llm rlvr acceleration, 2026. URL https://arxiv.org/abs/2604.11446.

Ganqu Cui, Lifan Yuan, Zefan Wang, Hanbin Wang, Yuchen Zhang, Jiacheng Chen, Wendi Li, Bingxiang He, Yuchen Fan, Tianyu Yu, Qixin Xu, Weize Chen, Jiarui Yuan, Huayu Chen, Kaiyan Zhang, Xingtai Lv, Shuo Wang, Yuan Yao, Xu Han, Hao Peng, Yu Cheng, Zhiyuan Liu, Maosong Sun, Bowen Zhou, and Ning Ding. Process reinforcement through implicit rewards, 2025a. URL https://arxiv.org/abs/2502.01456.

Ganqu Cui, Yuchen Zhang, Jiacheng Chen, Lifan Yuan, Zhi Wang, Yuxin Zuo, Haozhan Li, Yuchen Fan, Huayu Chen, Weize Chen, Zhiyuan Liu, Hao Peng, Lei Bai, Wanli Ouyang, Yu Cheng, Bowen Zhou, and Ning Ding. The entropy mechanism of reinforcement learning for reasoning language models, 2025b. URL https://arxiv.org/abs/2505.22617.

DeepSeek-AI. Deepseek-v4: Towards efficient long-context reasoning with hybrid attention and manifold hyperconnections. https://huggingface.co/deepseek-ai/DeepSeek-V4-Pro/blob/main/DeepSeek_V4.pdf, 4 2026. Accessed: 2026-04-24.

DeepSeek-AI, Daya Guo, Dejian Yang, Haowei Zhang, Junxiao Song, Ruoyu Zhang, Runxin Xu, Qihao Zhu, Shirong Ma, Peiyi Wang, Xiao Bi, Xiaokang Zhang, Xingkai Yu, Yu Wu, Z. F. Wu, Zhibin Gou, Zhihong Shao, Zhuoshu Li, Ziyi Gao, Aixin Liu, Bing Xue, Bingxuan Wang, Bochao Wu, Bei Feng, Chengda Lu, Chenggang Zhao, Chengqi Deng, Chenyu Zhang, Chong Ruan, Damai Dai, Deli Chen, Dongjie Ji, Erhang Li, Fangyun Lin, Fucong Dai, Fuli Luo, Guangbo Hao, Guanting Chen, Guowei Li, H. Zhang, Han Bao, Hanwei Xu, Haocheng Wang, Honghui Ding, Huajian Xin, Huazuo Gao, Hui Qu, Hui Li, Jianzhong Guo, Jiashi Li, Jiawei Wang, Jingchang Chen, Jingyang Yuan, Junjie Qiu, Junlong Li, J. L. Cai, Jiaqi Ni, Jian Liang, Jin Chen, Kai Dong, Kai Hu, Kaige Gao, Kang Guan, Kexin Huang, Kuai Yu, Lean Wang, Lecong Zhang, Liang Zhao, Litong Wang, Liyue Zhang, Lei Xu, Leyi Xia, Mingchuan Zhang, Minghua Zhang, Minghui Tang, Meng Li, Miaojun Wang, Mingming Li, Ning Tian, Panpan Huang, Peng Zhang, Qiancheng Wang, Qinyu Chen, Qiushi Du, Ruiqi Ge, Ruisong Zhang, Ruizhe Pan, Runji Wang, R. J. Chen, R. L. Jin, Ruyi Chen, Shanghao Lu, Shangyan Zhou, Shanhuang Chen, Shengfeng Ye, Shiyu Wang,

Shuiping Yu, Shunfeng Zhou, Shuting Pan, S. S. Li, Shuang Zhou, Shaoqing Wu, Shengfeng Ye, Tao Yun, Tian Pei, Tianyu Sun, T. Wang, Wangding Zeng, Wanjia Zhao, Wen Liu, Wenfeng Liang, Wenjun Gao, Wenqin Yu, Wentao Zhang, W. L. Xiao, Wei An, Xiaodong Liu, Xiaohan Wang, Xiaokang Chen, Xiaotao Nie, Xin Cheng, Xin Liu, Xin Xie, Xingchao Liu, Xinyu Yang, Xinyuan Li, Xuecheng Su, Xuheng Lin, X. Q. Li, Xiangyue Jin, Xiaojin Shen, Xiaosha Chen, Xiaowen Sun, Xiaoxiang Wang, Xinnan Song, Xinyi Zhou, Xianzu Wang, Xinxia Shan, Y. K. Li, Y. Q. Wang, Y. X. Wei, Yang Zhang, Yanhong Xu, Yao Li, Yao Zhao, Yaofeng Sun, Yaohui Wang, Yi Yu, Yichao Zhang, Yifan Shi, Yiliang Xiong, Ying He, Yishi Piao, Yisong Wang, Yixuan Tan, Yiyang Ma, Yiyuan Liu, Yongqiang Guo, Yuan Ou, Yuduan Wang, Yue Gong, Yuheng Zou, Yujia He, Yunfan Xiong, Yuxiang Luo, Yuxiang You, Yuxuan Liu, Yuyang Zhou, Y. X. Zhu, Yanhong Xu, Yanping Huang, Yaohui Li, Yi Zheng, Yuchen Zhu, Yunxian Ma, Ying Tang, Yukun Zha, Yuting Yan, Z. Z. Ren, Zehui Ren, Zhangli Sha, Zhe Fu, Zhean Xu, Zhenda Xie, Zhengyan Zhang, Zhewen Hao, Zhicheng Ma, Zhigang Yan, Zhiyu Wu, Zihui Gu, Zijia Zhu, Zijun Liu, Zilin Li, Ziwei Xie, Ziyang Song, Zizheng Pan, Zhen Huang, Zhipeng Xu, Zhongyu Zhang, and Zhen Zhang. Deepseek-r1: Incentivizing reasoning capability in llms via reinforcement learning, 2025. URL https://arxiv.org/abs/2501.12948.

Carl Eckart and Gale Young. The approximation of one matrix by another of lower rank. *Psychometrika*, 1:211–218, 1936. URL https://api.semanticscholar.org/CorpusID:10163399.

Yuqian Fu, Haohuan Huang, Kaiwen Jiang, Yuanheng Zhu, and Dongbin Zhao. Revisiting on-policy distillation: Empirical failure modes and simple fixes. *arXiv preprint arXiv:2603.25562*, 2026.

Mor Geva, Roei Schuster, Jonathan Berant, and Omer Levy. Transformer feed-forward layers are key-value memories, 2021. URL https://arxiv.org/abs/2012.14913.

Mor Geva, Avi Caciularu, Kevin Ro Wang, and Yoav Goldberg. Transformer feed-forward layers build predictions by promoting concepts in the vocabulary space, 2022. URL https://arxiv.org/abs/2203.14680.

Mor Geva, Jasmijn Bastings, Katja Filippova, and Amir Globerson. Dissecting recall of factual associations in auto-regressive language models, 2023. URL https://arxiv.org/abs/2304.14767.

Bingxiang He, Zekai Qu, Zeyuan Liu, Yinghao Chen, Yuxin Zuo, Cheng Qian, Kaiyan Zhang, Weize Chen, Chaojun Xiao, Ganqu Cui, Ning Ding, and Zhiyuan Liu. Justrl: Scaling a 1.5b llm with a simple rl recipe, 2025a. URL https://arxiv.org/abs/2512.16649.

Bingxiang He, Yuxin Zuo, Zeyuan Liu, Shangziqi Zhao, Zixuan Fu, Junlin Yang, Cheng Qian, Kaiyan Zhang, Yuchen Fan, Ganqu Cui, et al. How far can unsupervised rlvr scale llm training? *arXiv preprint arXiv:2603.08660*, 2026.

Zhiwei He, Tian Liang, Jiahao Xu, Qiuzhi Liu, Xingyu Chen, Yue Wang, Linfeng Song, Dian Yu, Zhenwen Liang, Wenxuan Wang, Zhuosheng Zhang, Rui Wang, Zhaopeng Tu, Haitao Mi, and Dong Yu. Deepmath-103k: A large-scale, challenging, decontaminated, and verifiable mathematical dataset for advancing reasoning, 2025b. URL https://arxiv.org/abs/2504.11456.

Jian Hu, Mingjie Liu, Ximing Lu, Fang Wu, Zaid Harchaoui, Shizhe Diao, Yejin Choi, Pavlo Molchanov, Jun Yang, Jan Kautz, and Yi Dong. Brorl: Scaling reinforcement learning via broadened exploration. *ArXiv*, abs/2510.01180, 2025a. URL https://api.semanticscholar.org/CorpusID:281705585.

Jingcheng Hu, Yinmin Zhang, Qi Han, Daxin Jiang, Xiangyu Zhang, and Heung-Yeung Shum. Open-reasoner-zero: An open source approach to scaling up reinforcement learning on the base model, 2025b. URL https://arxiv.org/abs/2503.24290.

Devvrit Khatri, Lovish Madaan, Rishabh Tiwari, Rachit Bansal, Sai Surya Duvvuri, Manzil Zaheer, Inderjit S Dhillon, David Brandfonbrener, and Rishabh Agarwal. The art of scaling reinforcement learning compute for llms. *arXiv preprint arXiv:2510.13786*, 2025.

Jeonghye Kim, Xufang Luo, Minbeom Kim, Sangmook Lee, Dohyung Kim, Jiwon Jeon, Dongsheng Li, and Yuqing Yang. Why does self-distillation (sometimes) degrade the reasoning capability of llms? 2026. URL https://api.semanticscholar.org/CorpusID:286776340.

Yehuda Koren, Robert Bell, and Chris Volinsky. Matrix factorization techniques for recommender systems. *Computer*, 42(8):30–37, 2009. doi: 10.1109/MC.2009.263.

Yaxuan Li, Yuxin Zuo, Bingxiang He, Jinqian Zhang, Chaojun Xiao, Cheng Qian, Tianyu Yu, Huanang Gao, Wenkai Yang, Zhiyuan Liu, et al. Rethinking on-policy distillation of large language models: Phenomenology, mechanism, and recipe. *arXiv preprint arXiv:2604.13016*, 2026.

Hunter Lightman, Vineet Kosaraju, Yura Burda, Harri Edwards, Bowen Baker, Teddy Lee, Jan Leike, John Schulman, Ilya Sutskever, and Karl Cobbe. Let's verify step by step. *arXiv preprint arXiv:2305.20050*, 2023.

Jiawei Liu, Chunqiu Steven Xia, Yuyao Wang, and Lingming Zhang. Is your code generated by chatgpt really correct? rigorous evaluation of large language models for code generation, 2023. URL https://arxiv.org/abs/2305.01210.

Mingjie Liu, Shizhe Diao, Ximing Lu, Jian Hu, Xin Dong, Yejin Choi, Jan Kautz, and Yi Dong. Prorl: Prolonged reinforcement learning expands reasoning boundaries in large language models. *ArXiv*, abs/2505.24864, 2025. URL https://api.semanticscholar.org/CorpusID:279071277.

Roy Mathias. The spectral norm of a nonnegative matrix. *Linear Algebra and its Applications*, 139: 269–284, 1990. ISSN 0024-3795. doi: https://doi.org/10.1016/0024-3795(90)90403-Y. URL https://www.sciencedirect.com/science/article/pii/002437959090403Y.

Kevin Meng, David Bau, Alex Andonian, and Yonatan Belinkov. Locating and editing factual associations in gpt, 2023. URL https://arxiv.org/abs/2202.05262.

OpenAI. Introducing gpt-oss. https://openai.com/zh-Hans-CN/index/introducing-gpt-oss/, 2025.

Qwen, :, An Yang, Baosong Yang, Beichen Zhang, Binyuan Hui, Bo Zheng, Bowen Yu, Chengyuan Li, Dayiheng Liu, Fei Huang, Haoran Wei, Huan Lin, Jian Yang, Jianhong Tu, Jianwei Zhang, Jianxin Yang, Jiaxi Yang, Jingren Zhou, Junyang Lin, Kai Dang, Keming Lu, Keqin Bao, Kexin Yang, Le Yu, Mei Li, Mingfeng Xue, Pei Zhang, Qin Zhu, Rui Men, Runji Lin, Tianhao Li, Tianyi Tang, Tingyu Xia, Xingzhang Ren, Xuancheng Ren, Yang Fan, Yang Su, Yichang Zhang, Yu Wan, Yuqiong Liu, Zeyu Cui, Zhenru Zhang, and Zihan Qiu. Qwen2.5 technical report, 2025. URL https://arxiv.org/abs/2412.15115.

Olivier Roy and Martin Vetterli. The effective rank: A measure of effective dimensionality. pp. 606–610, 2007. URL https://infoscience.epfl.ch/handle/20.500.14299/10320.

Guangming Sheng, Chi Zhang, Zilingfeng Ye, Xibin Wu, Wang Zhang, Ru Zhang, Yanghua Peng, Haibin Lin, and Chuan Wu. Hybridflow: A flexible and efficient rlhf framework. In *Proceedings of the Twentieth European Conference on Computer Systems*, EuroSys '25, pp. 1279–1297. ACM, March 2025. doi: 10.1145/3689031.3696075. URL http://dx.doi.org/10.1145/3689031.3696075.

Songting Shi. Visualizing data using gtsne, 2021. URL https://arxiv.org/abs/2108.01301.

Oscar Skean, Md Rifat Arefin, Dan Zhao, Niket Patel, Jalal Naghiyev, Yann LeCun, and Ravid Shwartz-Ziv. Layer by layer: Uncovering hidden representations in language models. *arXiv preprint arXiv:2502.02013*, 2025.

Mingyang Song and Mao Zheng. A survey of on-policy distillation for large language models. *arXiv preprint arXiv:2604.00626*, 2026.

Zelin Tan, Hejia Geng, Xiaohang Yu, Mulei Zhang, Guancheng Wan, Yifan Zhou, Qiang He, Xiangyuan Xue, Heng Zhou, Yutao Fan, Zhongzhi Li, Zaibin Zhang, Guibin Zhang, Chen Zhang, Zhenfei Yin, Philip Torr, and Lei Bai. Scaling behaviors of llm reinforcement learning post-training: An empirical study in mathematical reasoning, 2026. URL https://arxiv.org/abs/2509.25300.

Vatsal Venkatkrishna, Indraneil Paul, and Iryna Gurevych. Aletheia: What makes rlvr for code verifiers tick? *ArXiv*, abs/2601.12186, 2026. URL https://api.semanticscholar.org/CorpusID:284911417.

Jesse Vig, Sebastian Gehrmann, Yonatan Belinkov, Sharon Qian, Daniel Nevo, Yaron Singer, and Stuart Shieber. Investigating gender bias in language models using causal mediation analysis. *Advances in neural information processing systems*, 33:12388–12401, 2020.

Bangjun Xiao, Bingquan Xia, Bo Yang, Bofei Gao, Bowen Shen, Chen Zhang, Chenhong He, Chiheng Lou, Fuli Luo, Gang Wang, et al. Mimo-v2-flash technical report. *arXiv preprint arXiv:2601.02780*, 2026.

Yuanda Xu, Hejian Sang, Zhengze Zhou, Ran He, Zhipeng Wang, and Alborz Geramifard. Tip: Token importance in on-policy distillation. *arXiv preprint arXiv:2604.14084*, 2026.

An Yang, Anfeng Li, Baosong Yang, Beichen Zhang, Binyuan Hui, Bo Zheng, Bowen Yu, Chang Gao, Chengen Huang, Chenxu Lv, Chujie Zheng, Dayiheng Liu, Fan Zhou, Fei Huang, Feng Hu, Hao Ge, Haoran Wei, Huan Lin, Jialong Tang, Jian Yang, Jianhong Tu, Jianwei Zhang, Jianxin Yang, Jiaxi Yang, Jing Zhou, Jingren Zhou, Junyang Lin, Kai Dang, Keqin Bao, Kexin Yang, Le Yu, Lianghao Deng, Mei Li, Mingfeng Xue, Mingze Li, Pei Zhang, Peng Wang, Qin Zhu, Rui Men, Ruize Gao, Shixuan Liu, Shuang Luo, Tianhao Li, Tianyi Tang, Wenbiao Yin, Xingzhang Ren, Xinyu Wang, Xinyu Zhang, Xuancheng Ren, Yang Fan, Yang Su, Yichang Zhang, Yinger Zhang, Yu Wan, Yuqiong Liu, Zekun Wang, Zeyu Cui, Zhenru Zhang, Zhipeng Zhou, and Zihan Qiu. Qwen3 technical report, 2025. URL https://arxiv.org/abs/2505.09388.

Wenkai Yang, Weijie Liu, Ruobing Xie, Kai Yang, Saiyong Yang, and Yankai Lin. Learning beyond teacher: Generalized on-policy distillation with reward extrapolation. *ArXiv*, abs/2602.12125, 2026a. URL https://api.semanticscholar.org/CorpusID:285540530.

Wenkai Yang, Weijie Liu, Ruobing Xie, Kai Yang, Saiyong Yang, and Yankai Lin. Learning beyond teacher: Generalized on-policy distillation with reward extrapolation. *arXiv preprint arXiv:2602.12125*, 2026b.

Yixin Ye, Zhen Huang, Yang Xiao, Ethan Chern, Shijie Xia, and Pengfei Liu. Limo: Less is more for reasoning, 2025. URL https://arxiv.org/abs/2502.03387.

Qiying Yu, Zheng Zhang, Ruofei Zhu, Yufeng Yuan, Xiaochen Zuo, Yu Yue, Weinan Dai, Tiantian Fan, Gaohong Liu, Lingjun Liu, Xin Liu, Haibin Lin, Zhiqi Lin, Bole Ma, Guangming Sheng, Yuxuan Tong, Chi Zhang, Mofan Zhang, Wang Zhang, Hang Zhu, Jinhua Zhu, Jiaze Chen, Jiangjie Chen, Chengyi Wang, Hongli Yu, Yuxuan Song, Xiangpeng Wei, Hao Zhou, Jingjing Liu, Wei-Ying Ma, Ya-Qin Zhang, Lin Yan, Mu Qiao, Yonghui Wu, and Mingxuan Wang. Dapo: An open-source llm reinforcement learning system at scale, 2025. URL https://arxiv.org/abs/2503.14476.

Yang Yue, Zhiqi Chen, Rui Lu, Andrew Zhao, Zhaokai Wang, Yang Yue, Shiji Song, and Gao Huang. Does reinforcement learning really incentivize reasoning capacity in llms beyond the base model?, 2025. URL https://arxiv.org/abs/2504.13837.

Kaiyan Zhang, Yuxin Zuo, Bingxiang He, Youbang Sun, Runze Liu, Che Jiang, Yuchen Fan, Kai Tian, Guoli Jia, Pengfei Li, Yu Fu, Xingtai Lv, Yuchen Zhang, Sihang Zeng, Shang Qu, Haozhan Li, Shijie Wang, Yuru Wang, Xi-Dai Long, Fangfu Liu, Xiang Xu, Jiaze Ma, Xuekai Zhu, Ermo Hua, Yihao Liu, Zonglin Li, Hua yong Chen, Xiaoye Qu, Yafu Li, Weize Chen, Zhenzhao Yuan, Junqi Gao, Dong Li, Zhiyuan Ma, Ganqu Cui, Zhiyuan Liu, Biqing Qi, Ning Ding, and Bowen Zhou. A survey of reinforcement learning for large reasoning models. *ArXiv*, abs/2509.08827, 2025a. URL https://api.semanticscholar.org/CorpusID:281247204.

Kaiyan Zhang, Yuxin Zuo, Bingxiang He, Youbang Sun, Runze Liu, Che Jiang, Yuchen Fan, Kai Tian, Guoli Jia, Pengfei Li, Yu Fu, Xingtai Lv, Yuchen Zhang, Sihang Zeng, Shang Qu, Haozhan Li, Shijie Wang, Yuru Wang, Xinwei Long, Fangfu Liu, Xiang Xu, Jiaze Ma, Xuekai Zhu, Ermo Hua, Yihao Liu, Zonglin Li, Huayu Chen, Xiaoye Qu, Yafu Li, Weize Chen, Zhenzhao Yuan, Junqi Gao, Dong Li, Zhiyuan Ma, Ganqu Cui, Zhiyuan Liu, Biqing Qi, Ning Ding, and Bowen Zhou. A survey of reinforcement learning for large reasoning models, 2025b. URL https://arxiv.org/abs/2509.08827.

Shengyu Zhang, Linfeng Dong, Xiaoya Li, Sen Zhang, Xiaofei Sun, Shuhe Wang, Jiwei Li, Runyi Hu, Tianwei Zhang, Fei Wu, and Guoyin Wang. Instruction tuning for large language models: A survey, 2025c. URL https://arxiv.org/abs/2308.10792.

Zhihua Zhang. The singular value decomposition, applications and beyond, 2015. URL https://arxiv.org/abs/1510.08532.

Chujie Zheng, Kai Dang, Bowen Yu, Mingze Li, Huiqiang Jiang, Junrong Lin, Yuqiong Liu, Hao Lin, Chencan Wu, Feng Hu, An Yang, Jingren Zhou, and Junyang Lin. Stabilizing reinforcement learning with llms: Formulation and practices, 2025. URL https://arxiv.org/abs/2512.01374.

A Impact Statement

This paper presents work whose goal is to advance the understanding and efficiency of post-training for large language models, particularly on-policy distillation. We believe that our work conforms with the NeurIPS Code of Ethics. The proposed analysis and EffOPD method may help reduce the computational cost of post-training and make efficient model improvement more accessible. However, more efficient post-training techniques could also be misused to enhance or adapt models for harmful applications. We encourage responsible use of these methods, together with appropriate safety evaluation and deployment safeguards.

B Related Work

On-policy Distillation (OPD). In this paradigm, the student generates its own samples and receives dense supervisory signals from the teacher (Agarwal et al., 2024a). Qwen3 (Yang et al., 2025) demonstrates that it achieves substantially higher training efficiency than RLVR. Meanwhile, MiMo-V2-Flash (Xiao et al., 2026) and Deepseek-V4 (DeepSeek-AI, 2026) integrate multiple teacher skills into a small model via multi-task on-policy distillation. Song & Zheng (2026) present the first systematic survey of OPD for large language models, proposing a unified f-divergence framework grounded in on-policy samples. Fu et al. (2026) prove that token-level OPD is biased relative to the sequence-level reverse-KL objective but has a tighter variance bound of $O(T^2)$ versus $O(T^4)$. Yang et al. (2026b) establish a theoretical equivalence between token-level distillation and RLVR. Li et al. (2026) systematically investigate the training dynamics of OPD and identify two necessary conditions for success: (i) the student and teacher must share compatible thinking patterns, and (ii) the teacher must offer genuinely novel capabilities beyond what the student has encountered during training.

Emergent Behaviors of On-Policy Training. Yue et al. (2025) investigated the differences in sampling between base models and RL-fine-tuned models, showing that RL improves sampling efficiency for pass@1 but does not directly enhance reasoning ability. Cui et al. (2025b) identified the phenomenon of "entropy collapse" in reinforcement learning, where rapid early convergence causes the model to become overly confident, prematurely degrading its exploratory capacity. Through systematic experiments across models of varying scales, Tan et al. (2026) reveal a power-law relationship between test loss, computational budget, and data volume during RL post-training of LLMs, demonstrating that larger models consistently exhibit superior learning efficiency. Cai et al. (2025) investigate RL from the perspective of parameter dynamics. They uncover two fundamental properties of RL-induced updates: Rank-1 dominance and Rank-1 linear dynamics. Based on these insights, their AlphaRL framework achieves $3\times$ training acceleration. Building on this, Chen et al. (2026) train a predictor that directly forecasts the evolution direction of subsequent optimization subspaces using the early Rank-1 subspace. Different from previous studies focusing on RL's low-rank trajectories, this work finds that OPD's efficiency advantage over RL stems from the unique synergy between modular redundancy suppression and early directional stabilization.

C Limitations and Future Work

Despite our identification of two properties of OPD, this study has several limitations. First, although these properties are validated from multiple perspectives, their applicability to more complex settings, such as multi-turn agent tasks and multimodal reasoning, remains to be further examined. These settings may introduce stronger distributional shifts and more complex teacher-student residual structures. Second, our theoretical analysis in Appendix is inherently local, characterizing OPD dynamics only in a neighborhood of the base model and therefore not fully capturing the global non-convex behavior of large-scale post-training.

These limitations point to several directions for future work. A more complete theory should account for the coupling between the distillation objective, the evolving on-policy distribution, and the spectral evolution of parameter updates. In addition, the early directional lock-in observed in OPD may serve as a useful diagnostic signal for monitoring post-training dynamics. Metrics such as directional alignment, spectral concentration, and update compactness could help assess training progress and stability, thereby supporting more adaptive and efficient on-policy distillation methods for large language models.

D Preliminaries and Experimental Setup

D.1 Preliminaries

In our experiments, we focus on the two training paradigms: Reinforcement Learning (Zhang et al., 2025a) and On-Policy Distillation (Kim et al., 2026). Let π_θ denote the policy model to be optimized.

Reinforcement Learning (RL). The RL objective can be formulated as:

$$J_{\text{RL}}(\theta) = \max_{\theta} \mathbb{E}_{x\sim\mathcal{D},\, y\sim\pi_\theta(\cdot|x)} \left[r(x,y) - \beta D_{\text{KL}}\big(\pi_\theta \,\|\, \pi_{\text{ref}}\big) \right], \tag{5}$$

where the trajectory $y = (y_1, \ldots, y_T)$ is sampled from the current policy π_θ, ensuring on-policy training. The function $r(x, y)$ measures the quality of response y to query x. In the Reinforcement Learning from Verifiable Rewards setting (RLVR) (Venkatkrishna et al., 2026), $r(x, y)$ is a deterministic verifiable reward (e.g., answer correctness or unit test passing), requiring no learned reward model. The term $D_{\text{KL}}(\pi_\theta \,\|\, \pi_{\text{ref}})$ is a KL constraint that prevents the policy from deviating too far from a reference model π_{ref}, with β controlling the constraint strength.

To optimize Eq. (5), policy gradient methods are commonly used, yielding the following gradient estimate:

$$\nabla_\theta J_{\text{RL}}(\theta) = \mathbb{E}_{x\sim\mathcal{D},\, y\sim\pi_\theta(\cdot|x)} \left[\sum_{t=1}^{T} A_t \nabla_\theta \log \pi_\theta(y_t \mid x, y_{<t}) \right], \tag{6}$$

where A_t is the advantage of token y_t relative to a baseline. In practice, the reward signal in RLVR is often sparse, as the policy only receives a reward upon completion of the full response.

On-Policy Distillation (OPD). OPD inherits the on-policy nature of policy training while leveraging dense supervisory signals from a teacher model, making it an efficient post-training paradigm (Yang et al., 2026a). The core idea is to let the student model π_θ generate its own trajectories y, and then minimize the reverse KL divergence between the student and a fixed teacher model π^* on these student-generated trajectories:

$$J_{\text{OPD}}(\theta) = \min_{\theta} \mathbb{E}_{x\sim\mathcal{D},\, y\sim\pi_\theta(\cdot|x)} \left[D_{\text{KL}}\big(\pi_\theta(y \mid x) \,\|\, \pi^*(y \mid x)\big) \right]. \tag{7}$$

Note that the trajectories y in Eq. (7) are sampled from the student policy π_θ itself, preserving the on-policy property. The corresponding gradient is:

$$\nabla_\theta J_{\text{OPD}}(\theta) = \mathbb{E}_{x\sim\mathcal{D},\, y\sim\pi_\theta(\cdot|x)} \left[\sum_{t=1}^{T} \sum_{t'=t}^{T} \Big(\log \pi_\theta(y_{t'} \mid x, y_{<t'}) - \log \pi^*(y_{t'} \mid x, y_{<t'}) \Big) \nabla_\theta \log \pi_\theta(y_t \mid x, y_{<t}) \right]. \tag{8}$$

In practice, following prior work, a common approximation sets the discount factor to zero, focusing on immediate token-level optimization:

$$\nabla_\theta J_{\text{OPD}}(\theta) \approx \mathbb{E}_{x\sim\mathcal{D},\, y\sim\pi_\theta(\cdot|x)} \left[\sum_{t=1}^{T} \Big(\log \pi_\theta(y_t \mid x, y_{<t}) - \log \pi^*(y_t \mid x, y_{<t}) \Big) \nabla_\theta \log \pi_\theta(y_t \mid x, y_{<t}) \right]. \tag{9}$$

This approximation provides a dense learning signal at every token position, enabling OPD to achieve significantly higher training efficiency compared to RLVR with its sparse reward signal.

D.2 Experimental Setup

Table 2: Summary of models considered in this study.

Base Model	RL Model	Algorithm	Open-Source
Qwen2.5-1.5B-Deepseek	JustRL (He et al., 2025a)	GRPO	Yes
Qwen2.5-1.5B-Deepseek	BroRL (Hu et al., 2025a)	PPO	Yes
Qwen2.5-1.5B-Deepseek	ProRL (Liu et al., 2025)	DAPO	Yes
Qwen3-4B-Non-Thinking	Qwen-4B-Non-Thinking-GRPO	GRPO	Yes
Qwen2.5-7B	Open-Reasoner-Zero (Hu et al., 2025b)	PPO	Yes
Qwen3-8B-Base	Qwen3-8B-PPO (Cai et al., 2025)	PPO	Yes
Qwen3-8B-Base	Qwen3-8B-DAPO (Cai et al., 2025)	DAPO	Yes
Qwen3-14B-Base	Qwen3-14B-Base-DAPO	DAPO	No
Qwen3-14B	Qwen3-14B-GRPO	GRPO	No
Qwen2.5-32B	DAPO-Qwen-32B (Yu et al., 2025)	DAPO	Yes

To ensure the generality of our findings, we conduct experiments across multiple model scales, ranging from 1.5B to 32B parameters. Our experimental models include publicly available pre-trained checkpoints (e.g., Qwen2.5-7B, Qwen3-4B, etc.), as well as models locally trained using the Verl framework. For RL methods, we consider three representative algorithms—PPO, GRPO, and DAPO—and apply them to models of varying scales. For all OPD student models reported in Table 2, the capability-aligned teacher is consistently the RL-tuned version of its own base model (i.e., the RL model listed in the same table); for Qwen3-8B-Base, we also use Qwen3-14B-Base-DAPO as the teacher to ensure the generality of our conclusions.

For models trained with reinforcement learning locally, we adapt our training codebase using `Verl` (Sheng et al., 2025) and follow the corresponding training setups. All methods share the same core configuration: the maximum prompt length is 2,048 tokens and the maximum response length is 20,480 tokens, yielding a total budget of 22,528 tokens. During training, each backward pass uses a mini-batch of 32 samples, and gradients are accumulated for 16 iterations before a single optimization step is performed, resulting in an effective batch size of 512 under `Float16` precision. Each prompt generates $n = 16$ outputs during rollout. The learning rate is set to 1×10^{-6} with warmup, and gradient clipping of 1.0 is applied. We monitor the average reward per training batch and terminate training once the reward fails to improve for five consecutive steps.

In addition to the unified configuration described above, each method adopts specific hyperparameter settings in our experiments. For **GRPO**, we set both the high and low clipping ratios to 0.2 and apply a KL loss with coefficient 0.001, following DeepSeek-AI et al. (2025). For **DAPO**, we employ techniques such as clip-higher, dynamic sampling, token-level policy gradient loss, and overlong reward shaping, and apply the recommended hyperparameters from Yu et al. (2025): the clipping ratios are set to $\epsilon_{\text{low}} = 0.2$ and $\epsilon_{\text{high}} = 0.28$, KL divergence terms are removed entirely. We perform RLVR training on Qwen3-14B-Base models using the DeepMath-103K (He et al., 2025b) and MATH-12K (Lightman et al., 2023) for training. For the Qwen3-14B models, we conduct rollout and training in their non-thinking mode and we employ the built-in chat template, specified as follows:

```
User:
{question}
Please reason step by step, and put your final answer within \boxed{}.
<think>
</think>
Assistant: {CoT}
```

For OPD, we follow the setting of Yang et al. (2026a). The maximum prompt length is 2,048 tokens and the maximum response length is 16,384 tokens, yielding a total budget of 18,432 tokens. The prompt batch size is 1,024, and each prompt generates $n = 1$ outputs during rollout. The learning rate is set to 1×10^{-6}, without warmup, and a total of 3 training epochs. The next page shows the OPD training command using the `verl` framework. All of our training runs are conducted on $8\times$ or $32\times$ H20 96GB GPUs.

OPD Training Command

```
python3 -m verl.trainer.main_ppo \
    algorithm.adv_estimator=grpo \
    algorithm.rollout_correction.rollout_is=token \
    algorithm.rollout_correction.rollout_is_threshold=5.0 \
    algorithm.rollout_correction.rollout_rs=null \
    algorithm.rollout_correction.bypass_mode=false \
    actor_rollout_ref.rollout.calculate_log_probs=true \
    data.train_files=/path/to/train.parquet \
    data.val_files=/path/to/val.parquet \
    data.train_batch_size=1024 \
    data.max_prompt_length=2048 \
    data.max_response_length=16384 \
    data.filter_overlong_prompts=True \
    data.truncation='error' \
    data.shuffle=True \
    data.seed=42 \
    data.return_raw_chat=True \
    +data.apply_chat_template_kwargs.enable_thinking=False \
    actor_rollout_ref.model.path=$MODEL_PATH \
    +actor_rollout_ref.ref.model.path=$TEACHER_MODEL_PATH \
    actor_rollout_ref.actor.optim.lr=1e-6 \
    actor_rollout_ref.actor.optim.lr_warmup_steps_ratio=0.0 \
    actor_rollout_ref.model.use_remove_padding=True \
    actor_rollout_ref.actor.policy_loss.only_reverse_kl_advantages=True \
    actor_rollout_ref.actor.ppo_mini_batch_size=1024 \
    actor_rollout_ref.actor.ppo_micro_batch_size_per_gpu=1 \
    actor_rollout_ref.actor.use_kl_loss=True \
    actor_rollout_ref.actor.kl_loss_coef=0 \
    actor_rollout_ref.actor.kl_loss_type=low_var_kl \
    actor_rollout_ref.actor.entropy_coeff=0 \
    actor_rollout_ref.actor.ppo_max_token_len_per_gpu=22000 \
    actor_rollout_ref.model.enable_gradient_checkpointing=True \
    actor_rollout_ref.actor.fsdp_config.param_offload=False \
    actor_rollout_ref.actor.fsdp_config.optimizer_offload=False \
    actor_rollout_ref.rollout.log_prob_micro_batch_size_per_gpu=1 \
    actor_rollout_ref.rollout.tensor_model_parallel_size=1 \
    actor_rollout_ref.rollout.name=vllm \
    actor_rollout_ref.rollout.gpu_memory_utilization=0.6 \
    actor_rollout_ref.rollout.n=1 \
    actor_rollout_ref.rollout.max_num_batched_tokens=22000 \
    actor_rollout_ref.rollout.temperature=1.0 \
    actor_rollout_ref.rollout.top_p=1.0 \
    actor_rollout_ref.rollout.val_kwargs.do_sample=True \
    actor_rollout_ref.rollout.val_kwargs.temperature=1.0 \
    actor_rollout_ref.rollout.val_kwargs.top_p=1.0 \
    actor_rollout_ref.rollout.val_kwargs.n=32 \
    actor_rollout_ref.ref.log_prob_micro_batch_size_per_gpu=1 \
    actor_rollout_ref.ref.fsdp_config.param_offload=True \
    algorithm.use_kl_in_reward=False \
    reward_model.reward_manager=naive \
    trainer.critic_warmup=0 \
    trainer.val_before_train=True \
    trainer.logger='["console","wandb"]' \
    trainer.log_val_generations=10 \
    trainer.project_name='on-policy-distillation' \
    trainer.experiment_name='on-policy-distillation' \
    trainer.n_gpus_per_node=8 \
    trainer.nnodes=4 \
    trainer.save_freq=2 \
    trainer.default_local_dir=/path/to/save/dir \
    trainer.test_freq=2 \
    trainer.total_epochs=3 $@
```

E Property 1 Additional Experiment

E.1 Additional Experiment

This section provides additional empirical evidence to further validate **Property 1 (Functional Redundancy Avoidance)** introduced in Section 2.

We begin by examining the scaling behavior across model sizes. Figure 8 presents the scaling results on final checkpoints for models ranging from 1.5B to 32B parameters. Across all scales, we observe a consistent pattern: OPD achieves reasoning performance comparable to that of RL while requiring substantially smaller parameter update norms. This result suggests that the functional efficiency of OPD is not a scale-specific artifact, but rather an intrinsic property that generalizes across model sizes. We attribute this behavior to OPD's ability to systematically suppress functionally redundant updates, thereby concentrating the update budget on more effective directions.

We next investigate whether this advantage persists across different reinforcement learning algorithms. Figure 9 extends the analysis to a broader set of RL methods. Across all examined algorithms, OPD consistently demonstrates superior parameter update efficiency throughout the training trajectory. This advantage holds regardless of the specific learning dynamics or convergence behavior of the teacher RL method, indicating that the efficiency gain arises from the structural properties of OPD updates rather than the choice of the underlying RL algorithm. Taken together, these results provide consistent cross-scale and cross-algorithm evidence that OPD achieves comparable or even superior reasoning performance with significantly improved parameter efficiency.

While the main text shows that embedding layer updates contribute negligibly to reasoning performance, it does not explicitly analyze their distributional shift relative to the base model. To address this, we sample reasoning sequences generated by the base model and extract their token embeddings. We then visualize the embedding shifts using PCA (Eckart & Young, 1936) and t-SNE (Shi, 2021), and quantify the distributional differences via cosine similarity between token representations. As shown in Figure 11 and Table 3, OPD consistently exhibits smaller embedding shifts than RL across all model scales, and maintains higher similarity to the base representations. These findings indicate that, despite their limited functional contribution, embedding layers in OPD still undergo more constrained and compact updates, effectively avoiding the unnecessary drift commonly observed in RL. This suggests that OPD enforces compact updates not only in critical modules but also in functionally peripheral regions.

Finally, we validate the component-level properties identified in the main text under a broader range of datasets and algorithmic settings. These properties include the negligible contribution of embedding layers, the functional dominance of middle-layer MLPs, and the consistent redundancy suppression pattern across architectural components. As shown in Figure 10, the results consistently support these observations, further reinforcing that Property 1 reflects an intrinsic and stable characteristic of OPD's parameter update dynamics, rather than an artifact of specific experimental conditions.

E.2 Detailed Setup of Sliding-Window Intervention Analysis

This section provides a formal description of the sliding-window intervention analysis used in Section 2.2. The goal of this analysis is to localize the contribution of parameter updates across different layers and modules (Cai et al., 2024, 2025), and to examine whether redundant updates in reinforcement learning (RL) are primarily concentrated in functionally non-critical regions.

The core idea of this method is to inject parameter updates into localized regions of the network and measure the resulting performance change (Meng et al., 2023; Vig et al., 2020). Compared to full-model replacement, this localized intervention allows us to isolate the marginal functional contribution of updates at different depths, thereby enabling a fine-grained characterization of the relationship between update location and functional impact.

We consider a Transformer model with L layers, where each layer consists of two core modules: Attention and MLP. Let $\Delta W_{\text{RL/OPD}}^{(i,\text{Attn})}$ and $\Delta W_{\text{RL/OPD}}^{(i,\text{MLP})}$ denote the parameter updates of the Attention and MLP modules at layer i, respectively.

For a target layer l, we define the sliding window as:

$$\mathcal{W}_l = \{i \in \mathbb{Z} \mid \max(1,\, l-8) \le i \le \min(L,\, l+8)\}\,. \tag{10}$$

The window is centered at layer l and extends 8 layers to both sides, resulting in a maximum width of 17 layers. Near the model boundaries, the window is truncated accordingly. This design balances locality and stability: by covering neighboring layers, it mitigates the high variance associated with single-layer interventions while preserving spatial resolution.

To isolate the independent contributions of MLP and Attention modules, we construct two types of intervened models. In each setting, only the parameters of the specified module within the sliding window are replaced, while all other parameters are fixed to those of the base model.

MLP Intervention:

$$W_{\text{MLP},l}^{(\text{interv})} = \begin{cases} W_{\text{Base}}^{(i,\text{MLP})} + \Delta W_{\text{RL/OPD}}^{(i,\text{MLP})}, & i \in \mathcal{W}_l \\ W_{\text{Base}}^{(i,\text{MLP})}, & i \notin \mathcal{W}_l. \end{cases} \tag{11}$$

All Attention parameters are fixed to $W_{\text{Base}}^{(i,\text{Attn})}$.

Attention Intervention:

$$W_{\text{Attn},l}^{(\text{interv})} = \begin{cases} W_{\text{Base}}^{(i,\text{Attn})} + \Delta W_{\text{RL/OPD}}^{(i,\text{Attn})}, & i \in \mathcal{W}_l \\ W_{\text{Base}}^{(i,\text{Attn})}, & i \notin \mathcal{W}_l. \end{cases} \tag{12}$$

All MLP parameters are fixed to $W_{\text{Base}}^{(i,\text{MLP})}$.

This intervention strategy effectively constructs a *local update injection – global performance response* analysis framework, allowing us to attribute overall performance changes to specific layers and modules, and thereby reveal the functional distribution of parameter updates across the network.

In practice, we iterate over all valid window centers $l = 1, 2, \ldots, L-8$, construct the two types of intervened models for each l, and evaluate their accuracy on MATH500 (Lightman et al., 2023). Each intervened model is evaluated using four independent forward passes, and the results are averaged to reduce evaluation noise.

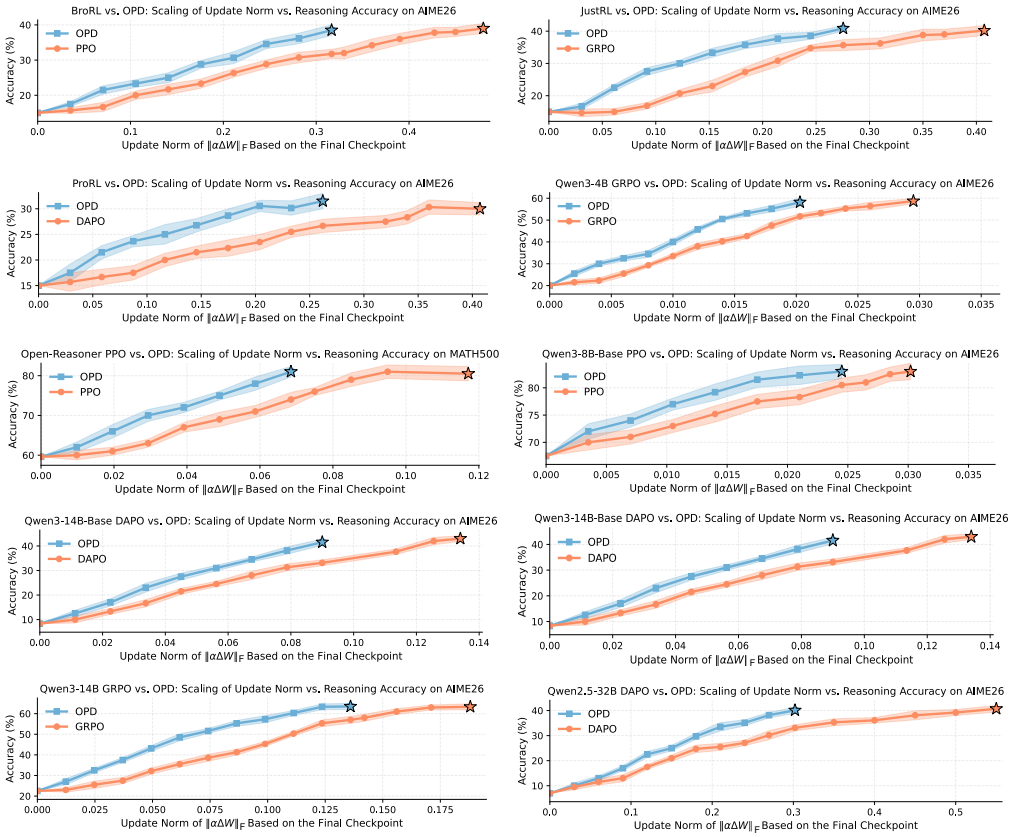

Figure 8: Comparison of parameter update efficiency between RL and OPD. Scaling analysis of the final checkpoints demonstrates that OPD achieves substantially higher reasoning gains than RL under an identical update norm budget.

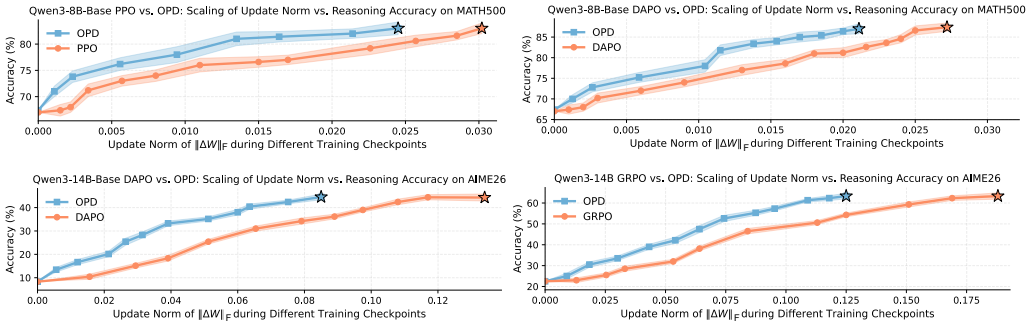

Figure 9: Comparison of parameter update efficiency between RL and OPD. Analysis of intermediate checkpoints throughout training demonstrates that OPD achieves the same reasoning accuracy as RL with substantially smaller parameter update norms.

Figure 10: Functional contributions and update distributions across architectural components. (a) Effect of embedding layer replacement on MATH500. (b) Layer-wise update norms (bars, left axis) for RL/OPD-trained Qwen3-8B-Base models, and corresponding **RL** reasoning accuracy after sliding-window intervention (line, right axis) on MATH500.

Table 3: Cosine similarity between RL/OPD with Base model token embeddings.

Base Model	**Model**	**Cosine Sim.**
Qwen2.5-1.5B-Deepseek	JustRL (He et al., 2025a)	0.9156
	OPD	0.9412
Qwen2.5-1.5B-Deepseek	BroRL (Hu et al., 2025a)	0.9078
	OPD	0.9371
Qwen2.5-1.5B-Deepseek	ProRL (Liu et al., 2025)	0.9287
	OPD	0.9514
Qwen3-4B	Qwen-4B-GRPO (Yang et al., 2026a)	0.9672
	OPD	0.9851
Qwen3-8B-Base	Qwen3-8B-DAPO (Cai et al., 2025)	0.9421
	OPD	0.9752
Qwen3-14B-Base	Qwen3-14B-Base-DAPO	0.8961
	OPD	0.9512

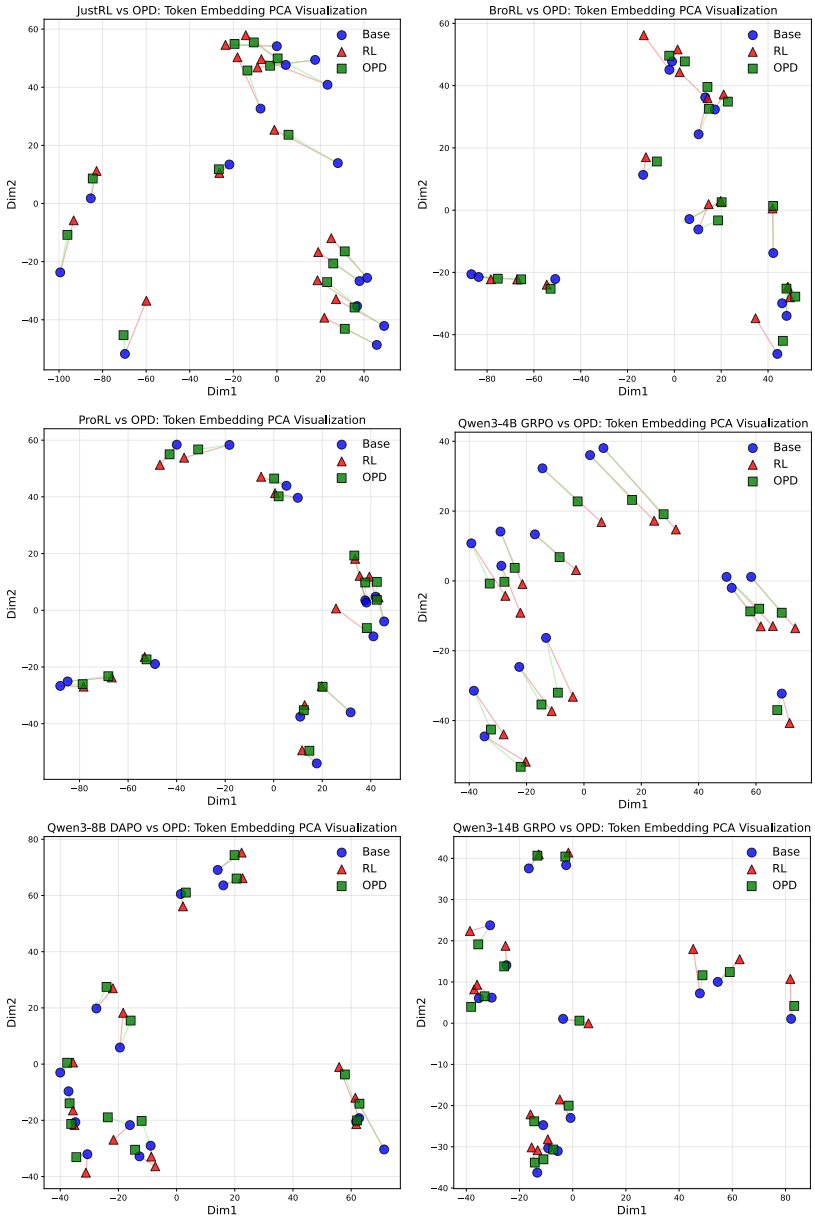

Figure 11: t-SNE visualization of token embeddings from the Base, RL, and OPD models. The red and green lines indicate the shifts from Base to RL and from Base to OPD, respectively.

F Property 2 Additional Experiment

F.1 Geometric Metrics for Parameter Update Matrix

In this section, we provide formal definitions of four complementary metrics used to characterize the geometric structure of the parameter update matrix $\Delta W \in \mathbb{R}^{m\times n}$. Let the singular value decomposition (SVD) of ΔW be:

$$\Delta W = U\Sigma V^\top, \quad \Sigma = \mathrm{diag}(\sigma_1, \sigma_2, \ldots, \sigma_r), \tag{13}$$

where $r = \mathrm{rank}(\Delta W)$ and $\sigma_1 \geq \sigma_2 \geq \cdots \geq \sigma_r > 0$ are the singular values sorted in descending order.

Spectral Norm (Mathias, 1990). The spectral norm is defined as the largest singular value σ_1.. This metric captures the magnitude of the update along the dominant direction in parameter space, corresponding to the maximum amplification induced by ΔW on any input vector.

Spectral-to-Frobenius Norm Ratio (Al-Natoor, 2024). The spectral-to-Frobenius norm ratio is defined as:

$$\rho = \frac{\sigma_1}{\sqrt{\sum_{j=1}^{r}\sigma_j^2}}. \tag{14}$$

This ratio quantifies the dominance of the leading singular direction. A value of ρ close to 1 indicates that the update is highly concentrated along a single direction, whereas smaller values suggest that the update energy is distributed across multiple directions.

Effective Rank (Roy & Vetterli, 2007). The effective rank, also referred to as the spectral entropy rank, is defined as:

$$\mathrm{rank}_{\mathrm{eff}} = \exp\left(-\sum_{i=1}^{r}\bar{\sigma}_i \log \bar{\sigma}_i\right), \tag{15}$$

where $\bar{\sigma}_i = \sigma_i / \sum_{j=1}^{r}\sigma_j$ denotes the normalized singular values. This metric measures the entropy of the singular value spectrum. A smaller effective rank indicates rapid spectral decay and concentration of update energy in a low-dimensional subspace, while a larger effective rank implies a more diffuse distribution.

Top-1% Subspace Norm Ratio (Cai et al., 2025). Let $k = \lceil r/100 \rceil$ denote the number of singular components corresponding to the Top 1% of the spectrum. We construct the rank-k approximation of ΔW using these leading components:

$$\Delta W_k = U_{:,1:k}\Sigma_{1:k,1:k}V^\top_{:,1:k}. \tag{16}$$

The Top-1% subspace norm ratio is defined as:

$$R_{\text{Top-1\%}} = \frac{\|\Delta W_k\|_F}{\|\Delta W\|_F} = \sqrt{\frac{\sum_{i=1}^{k}\sigma_i^2}{\sum_{j=1}^{r}\sigma_j^2}}. \tag{17}$$

This metric quantifies the fraction of the total update energy captured by the Top 1% of singular directions. A value close to 1 indicates that the update is effectively confined to an extremely low-dimensional subspace. For each model, we report the average values of the computed metrics across all MLP and attention matrices.

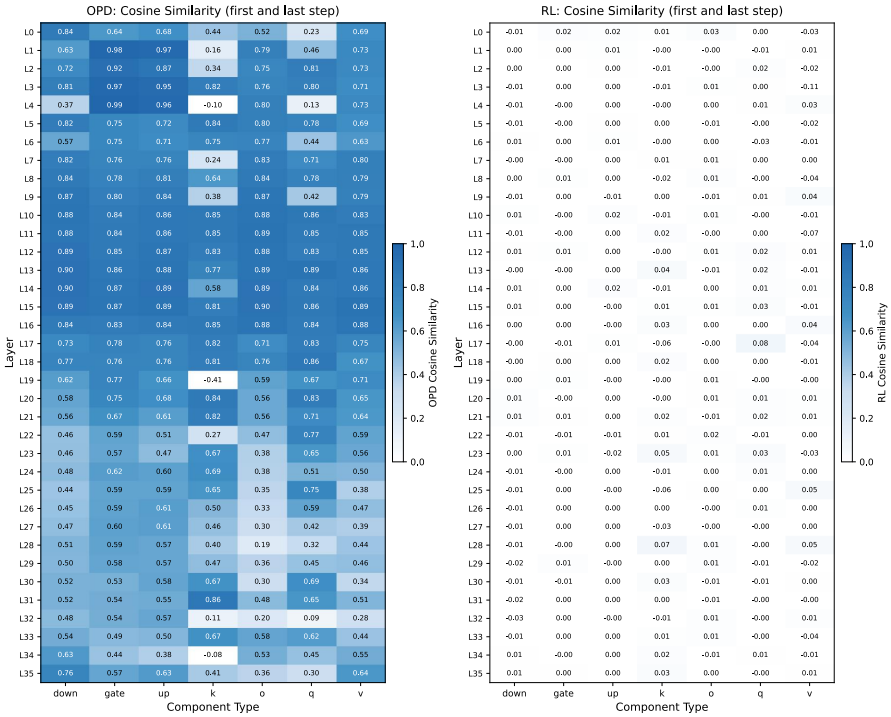

Figure 12: Heatmap of cosine-similarity of $\mathcal{U}_1$ at the first and last steps for each component trained under OPD and RL.

F.2 Cosine Similarity Analysis of Subspaces

This section provides additional empirical evidence for Property 2 (Early Low-Rank Lock-in) by analyzing the directional stability of dominant update subspaces during training. We focus on how the principal subspaces evolve from the early training stage to the final converged checkpoint, thereby characterizing the subspace-level convergence behavior of different training methods.

To this end, we perform singular value decomposition (SVD) on the parameter update matrix and analyze the dominant subspaces spanned by its leading singular vectors. Specifically, we consider the Rank-1 subspace $\mathcal{U}_1$, which corresponds to the strongest singular direction and captures the primary low-dimensional structure of update energy. We compute the cosine similarity between early-stage and final-stage subspaces to measure the degree of directional lock-in during training. The results are shown in Figure 12.

RL exhibits unstable dominant subspace evolution. During RL training, the cosine similarity between early-stage and final-stage subspaces remains consistently low across modules. This indicates that RL does not establish update directions aligned with the final checkpoint at the early stage. Instead, its dominant subspaces undergo substantial changes throughout training, suggesting that RL requires continuous exploration and correction before gradually converging to a stable configuration.

OPD exhibits early alignment of dominant subspaces. In contrast, OPD shows substantially higher subspace consistency across most modules. In particular, intermediate layers exhibit especially strong early alignment, with cosine similarity reaching up to 0.9. These results indicate that OPD identifies stable dominant update directions early in training, while subsequent optimization mainly amplifies the update magnitude along these directions rather than repeatedly searching for new directions.

This observation provides further support for Property 1 from a representational geometry perspective. As Property 1 indicates, OPD suppresses functionally redundant updates and concentrates parameter changes within reasoning-critical intermediate modules. The present subspace analysis elucidates the mechanistic basis for such compact updates: in these modules, the dominant update subspaces stabilize early during training, enabling OPD to amplify updates along these consistent directions while minimizing redundant parameter movement. Consequently, OPD achieves substantial performance

improvements with high parameter efficiency, as the optimization primarily reinforces already stable, task-relevant directions rather than exploring unnecessary or redundant dimensions.

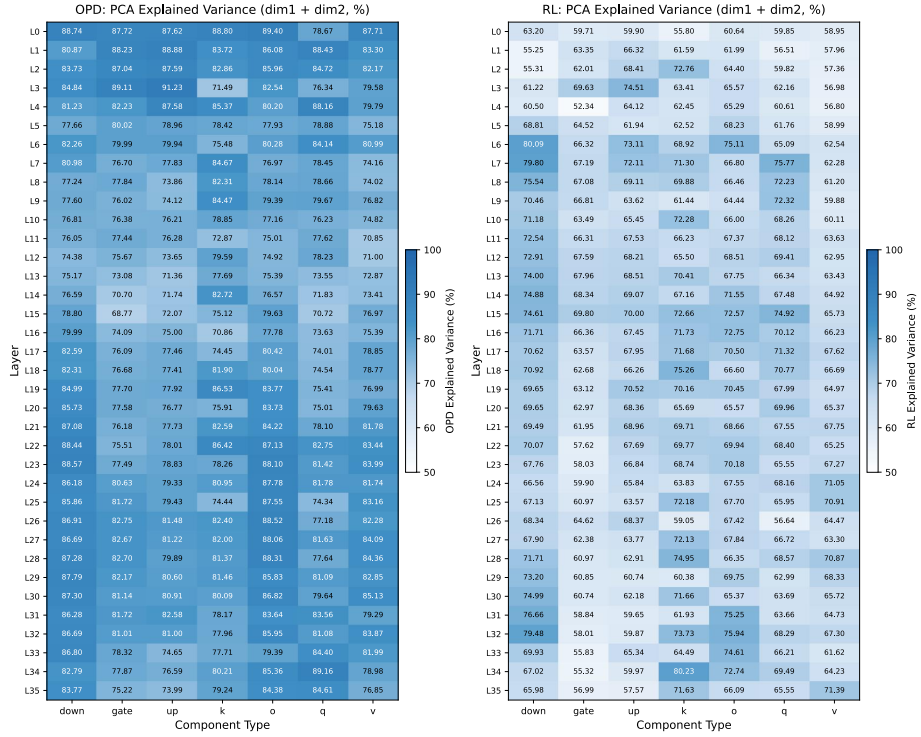

Figure 13: Heatmap of $\mathcal{U}_1$ trajectory under OPD and RL, along with variance explained by the first two dimensions after PCA.

F.3 Trajectory Evolution of Subspaces

Trajectory Visualization. Beyond similarity analysis, we further investigate the temporal evolution of dominant subspaces during training by visualizing the trajectories of Rank-1 subspaces $\mathcal{U}_1$ across different modules. Specifically, we apply t-SNE dimensionality reduction (Shi, 2021) to representations from different training checkpoints, with results shown in Figures 15-28.

We observe that OPD exhibits markedly more concentrated trajectory patterns: its evolution is confined to a narrower region in the projected space and follows a smoother, near-linear path. In contrast, RL trajectories are significantly more dispersed and irregular. This suggests that OPD induces stronger directional stability during representation evolution, resulting in a more structured and predictable optimization trajectory.

Quantitative Characterization via PCA. To quantify this phenomenon, we perform PCA (Eckart & Young, 1936) on representations from different training checkpoints. For each module, we collect the checkpoint-wise representation vectors and form a trajectory matrix $X \in \mathbb{R}^{T\times d}$, where T denotes the number of checkpoints and d is the representation dimension. After centering X, PCA decomposes the covariance matrix and obtains eigenvalues $\lambda_1 \geq \lambda_2 \geq \cdots \geq \lambda_d$. We then compute the cumulative variance explained by the first two principal components as

$$\mathrm{EVR}_{0:2} = \frac{\lambda_1 + \lambda_2}{\sum_{i=1}^{d} \lambda_i}. \tag{18}$$

This quantity measures how much of the trajectory variation across training checkpoints can be captured by a two-dimensional principal subspace. A higher value indicates that the trajectory is more concentrated and lower-dimensional, whereas a lower value suggests that the evolution is more dispersed across multiple directions. The results are summarized in Figure 13.

Overall, OPD consistently achieves substantially higher $\mathrm{EVR}_{0:2}$ than RL. This indicates that the OPD representations are more strongly concentrated within a low-dimensional and compact subspace during training. In contrast, RL representations distribute their variation across a broader set of directions, reflecting greater redundancy and less structured trajectory evolution.

Mechanistic Interpretation. Overall, these observations provide a unified geometric and information-theoretic perspective on the behaviors described in Property 1 and Property 2. Specifically, during training, the update dynamics are not evenly distributed across the high-dimensional parameter space but are highly concentrated along a few dominant directions forming a low-dimensional subspace. From an information-theoretic standpoint, this concentration acts as a form of implicit compression, enhancing parameter utilization efficiency (Property 1) while facilitating early stabilization of update directions (Property 2).

From the perspective of optimization geometry, this concentration reflects an implicit low-rank bias: under dense teacher supervision, OPD preferentially updates along a small number of stable and effective directions rather than exploring the high-dimensional parameter space indiscriminately. As a result, the parameter evolution exhibits a highly structured pattern, with both the direction and support of updates tightly constrained, yielding compact and stable trajectory evolution.

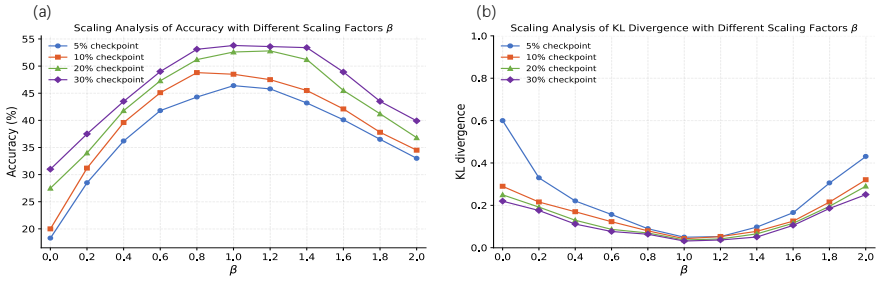

Figure 14: Scaling analysis of (a) accuracy and (b) KL divergence across different training checkpoints, with optimal performance achieved in the range $0.8 \leq \beta \leq 1.2$.

F.4 Scaling Effects on Accuracy and Distribution Alignment

This subsection aims to further validate and complement the findings in Section 3 Figure 5, focusing on the relationship between the magnitude of early updates and model performance.

Effect of Scaling Magnitude on Performance. To analyze the effect of scaling early checkpoint updates on model performance, we define the updated parameters after scaling as:

$$\Delta W_{\text{scaled}} = \Delta W_{\text{early}} + \underbrace{\Delta W_{\text{early}} \times \frac{\beta \cdot (\|\Delta W_{\text{final}}\|_F - \|\Delta W_{\text{early}}\|_F)}{\|\Delta W_{\text{early}}\|_F}}_{\text{extra update}}. \tag{19}$$

Here, β is the scaling coefficient. When $\beta = 0$, $\Delta W_{\text{scaled}} = \Delta W_{\text{early}}$, i.e., no extra update is added. When $\beta = 1$, $\|\Delta W_{\text{scaled}}\|_F = \|\Delta W_{\text{final}}\|_F$, i.e., the magnitude of the scaled update matches that of the final update.

As shown in Figure 14 (a), increasing β from 0 progressively improves model performance. When $\beta \approx 0.8$, the performance gain begins to plateau; when β exceeds a large value (approximately 1.2), performance starts to degrade. This trend provides three key insights: (i) the early checkpoint already captures a principal subspace aligned with the final solution, as evidenced by performance gains from moderate scaling; (ii) the plateau around $\beta \approx 0.8$ reflects inherent representational limits of the early subspace, indicating that further amplification cannot fully bridge the gap without additional training; (iii) excessive scaling leads to performance decline, suggesting that extra norm amplifies noise or irrelevant components, harming task performance.

Alignment with Teacher Distribution. To further understand these trends, we measure the KL divergence between the student's outputs and the teacher's distribution. Figure 14 (b) shows that KL divergence decreases monotonically with increasing β, stabilizes over the intermediate range corresponding to the performance plateau, and rises again for $\beta > 1.2$. These trends mirror the accuracy results: initially, monotonic KL reduction coincides with steady accuracy improvement, indicating that closer approximation to the teacher distribution directly drives task performance. Within the optimal range ($\beta \approx 0.8$–1.2), KL divergence remains low and accuracy saturates, demonstrating strong student-teacher distribution alignment.

This phenomenon can be interpreted from two complementary perspectives. First, from a causal inference viewpoint, KL reduction—i.e., more precise alignment with the teacher's behavioral distribution—directly drives improvements in task accuracy. Second, from the perspective of representation subspace geometry, the reduction in KL following scaling reveals that the early update directions already capture the dominant structure of the teacher's distribution. While the early subspace norm may initially be insufficient, its directions are largely aligned with the final converged solution. Appropriate scaling partially unlocks the representational capacity encoded in this subspace, thereby reducing the distributional gap between student and teacher.

Illustrative example of scaling-induced reasoning improvement. Then, we provide a concrete example to illustrate the differences in text representations between the early checkpoint and the

teacher model. On the next page, we compare the generated responses of the early checkpoint before and after scaling. Specifically, when we scale the norm of the early checkpoint to match that of the final model, the quality of its generated responses improves significantly compared to the unscaled version. Further analysis reveals that the scaled responses exhibit a noticeable increase in the number of reasoning steps, with each step becoming more fine-grained. The model demonstrates richer intermediate reasoning processes and clearer logical progression, rather than jumping directly to results. This change reflects reasoning habits that are more similar to those of the teacher model, indicating that appropriate norm scaling can activate the reasoning structures already encoded in the early subspace, making the student's generation behavior more akin to the teacher's in terms of reasoning depth and logical coherence.

F.5 A Local Geometric View of OPD Dynamics

In this subsection, we provide a local geometric analysis to explain why On-Policy Distillation (OPD) naturally induces low-rank and early-locked update directions, and how this differs from the update dynamics of reinforcement learning (RL). By linearizing the student model around the base model, we reveal how the structure of the OPD objective gives rise to the empirical phenomena observed in the main text.

Setup and Linearization. Let a token context be denoted by $c = (x, y_{<t})$, where x is the input prompt and $y_{<t}$ are previously generated tokens. Define:

- $z_\theta(c) \in \mathbb{R}^V$: logits of the student model with parameters θ (vocabulary size V).
- $z^\star(c) \in \mathbb{R}^V$: logits of a fixed teacher model.
- θ_0: parameters of the base model (initialization for both RL and OPD training).
- $\Delta\theta = \theta - \theta_0$: parameter displacement.

Expand $z_\theta(c)$ around θ_0 to first order:

$$z_\theta(c) = z_{\theta_0}(c) + \underbrace{\left.\frac{\partial z_\theta(c)}{\partial \theta}\right|_{\theta=\theta_0}}_{=:J_c} \Delta\theta + O(\|\Delta\theta\|^2). \tag{20}$$

Here $J_c \in \mathbb{R}^{V\times \dim(\theta)}$ is the Jacobian matrix of the logits with respect to the parameters. For sufficiently small step sizes and early training, $\|\Delta\theta\|$ is small, and we neglect the higher-order terms:

$$z_\theta(c) \approx z_0(c) + J_c\Delta\theta, \qquad \text{where } z_0(c) := z_{\theta_0}(c). \tag{21}$$

Define the *teacher-student logit residual at the base model*:

$$r_c := z^\star(c) - z_0(c). \tag{22}$$

Then the logit discrepancy becomes:

$$z_\theta(c) - z^\star(c) \approx J_c\Delta\theta - r_c. \tag{23}$$

Local Quadratic Approximation of the OPD Objective. The OPD objective minimizes the reverse KL divergence between the student and the teacher on on-policy samples:

$$\mathcal{L}_{\mathrm{OPD}}(\theta) = \mathbb{E}_{x\sim\mathcal{D},\, y\sim\pi_\theta(\cdot|x)}\left[D_{\mathrm{KL}}\big(\pi_\theta(\cdot|x, y_{<t}) \,\|\, \pi^\star(\cdot|x, y_{<t})\big)\right]. \tag{24}$$

For a fixed context c, denote:

$$p_\theta(\cdot|c) = \mathrm{softmax}(z_\theta(c)), \qquad p^\star(\cdot|c) = \mathrm{softmax}(z^\star(c)). \tag{25}$$

When the two distributions are close, the KL divergence admits a second-order Taylor expansion in the logit space. Let $f(z) = D_{\mathrm{KL}}(p_z\|p^\star)$ where $p_z = \mathrm{softmax}(z)$. Then:

$$f(z) \approx f(z^\star) + \underbrace{\nabla f(z^\star)^\top (z - z^\star)}_{=0} + \frac{1}{2}(z - z^\star)^\top \nabla^2 f(z^\star)(z - z^\star), \tag{26}$$

because the first derivative vanishes at $z = z^\star$ (minimum). The Hessian of the reverse KL at the teacher point is the Fisher information matrix of the student distribution:

$$\nabla^2 f(z^\star) = \mathrm{Diag}(p^\star) - p^\star {p^\star}^\top =: F_c^\star. \tag{27}$$

Thus, for z near $z^\star$:

$$D_{\mathrm{KL}}(p_z \| p^\star) \approx \frac{1}{2}(z - z^\star)^\top F_c^\star (z - z^\star). \tag{28}$$

However, in our local analysis we linearize around θ_0, so the student logits $z_\theta(c)$ are close to $z_0(c)$, not necessarily close to $z^\star(c)$. To obtain a quadratic form in $\Delta\theta$, we may evaluate the Fisher matrix at a convenient distribution, typically the base model distribution $p_0(c) = \mathrm{softmax}(z_0(c))$. This yields an approximation that is consistent when $z_\theta \approx z_0$ and the teacher is not too far from the base model. Define:

$$F_c := \mathrm{Diag}(p_0(c)) - p_0(c) p_0(c)^\top. \tag{29}$$

Then we approximate:

$$D_{\mathrm{KL}}(p_\theta \| p^\star) \approx \frac{1}{2}(z_\theta(c) - z^\star(c))^\top F_c (z_\theta(c) - z^\star(c)) = \frac{1}{2}(J_c \Delta\theta - r_c)^\top F_c (J_c \Delta\theta - r_c). \tag{30}$$

If the teacher and base model are already reasonably aligned (a common scenario in distillation), then $z^\star \approx z_0$ and $F_c \approx F_c^\star$. Even if not, the quadratic form still provides a local approximation of the KL divergence up to an additive constant, because:

$$D_{\mathrm{KL}}(p_\theta \| p^\star) = D_{\mathrm{KL}}(p_0 \| p^\star) + \nabla_\theta D_{\mathrm{KL}}(p_\theta \| p^\star)|_{\theta_0} \Delta\theta + \frac{1}{2}\Delta\theta^\top H \Delta\theta + \cdots, \tag{31}$$

and the Hessian at θ_0 involves $J_c^\top F_c^\star J_c$. Evaluating F_c at p_0 is a standard simplification in the neural tangent kernel literature and preserves the correct second-order structure when $\|z^\star - z_0\|$ is small.

Local Expected Objective and Gradient. Taking expectation over the on-policy contexts c which, to first order, can be approximated by the base model's distribution, we obtain:

$$\mathcal{L}_{\mathrm{OPD}}(\Delta\theta) \approx \frac{1}{2}\mathbb{E}_c\big[(J_c \Delta\theta - r_c)^\top F_c (J_c \Delta\theta - r_c)\big]. \tag{32}$$

Expanding the quadratic:

$$\mathcal{L}_{\mathrm{OPD}}(\Delta\theta) \approx \frac{1}{2}\Delta\theta^\top \underbrace{\mathbb{E}_c[J_c^\top F_c J_c]}_{=:A} \Delta\theta - \Delta\theta^\top \underbrace{\mathbb{E}_c[J_c^\top F_c r_c]}_{=:b} + \frac{1}{2}\mathbb{E}_c[r_c^\top F_c r_c]. \tag{33}$$

The last term is constant with respect to $\Delta\theta$. Therefore, the local objective is a convex quadratic:

$$\mathcal{L}_{\mathrm{OPD}}(\Delta\theta) = \frac{1}{2}\Delta\theta^\top A \Delta\theta - b^\top \Delta\theta + \text{const}. \tag{34}$$

The gradient with respect to $\Delta\theta$ is:

$$g(\Delta\theta) := \nabla_{\Delta\theta} \mathcal{L}_{\mathrm{OPD}} = A\Delta\theta - b. \tag{35}$$

Gradient Descent Dynamics and Closed-Form Solution. Consider gradient descent on $\Delta\theta$ with fixed step size $\eta > 0$:

$$\Delta\theta_{s+1} = \Delta\theta_s - \eta g(\Delta\theta_s) = \Delta\theta_s - \eta(A\Delta\theta_s - b) = (I - \eta A)\Delta\theta_s + \eta b. \tag{36}$$

Starting from $\Delta\theta_0 = 0$ (initialization at the base model), we unroll the recursion:

$$\Delta\theta_1 = \eta b, \tag{37}$$

$$\Delta\theta_2 = (I - \eta A)\eta b + \eta b = \eta[I + (I - \eta A)]b, \tag{38}$$

$$\Delta\theta_s = \eta \sum_{j=0}^{s-1} (I - \eta A)^j b. \tag{39}$$

This is a geometric series of matrices. Assume A is symmetric positive semidefinite (it is a Gram matrix of $J_c^\top F_c^{1/2}$). Choose η such that $0 < \eta < 2/\lambda_{\max}(A)$ to ensure convergence. Then $I - \eta A$ has spectral radius less than 1, and the series converges to:

$$\Delta\theta_\infty = \eta(I - (I - \eta A))^{-1} b = A^{-1} b, \tag{40}$$

where A^{-1} denotes the pseudo-inverse on the support of A. The finite-sum formula can be expressed in closed form:

$$\Delta\theta_s = \big[I - (I - \eta A)^s\big] A^{-1} b. \tag{41}$$

This is verified by factoring:

$$\sum_{j=0}^{s-1} (I - \eta A)^j = (I - (I - \eta A)^s)(I - (I - \eta A))^{-1} = (I - (I - \eta A)^s)(\eta A)^{-1}. \tag{42}$$

Multiplying by ηb gives the result.

Spectral Decomposition and Directional Dynamics. Let $A = U\Lambda U^\top$ be the eigen-decomposition with $\Lambda = \mathrm{diag}(\lambda_1, \lambda_2, \ldots, \lambda_d)$ and $\lambda_1 \geq \lambda_2 \geq \cdots \geq \lambda_d \geq 0$. Let $b = U\beta$ with $\beta_i = \langle b, u_i \rangle$. Since $A^{-1} = U\Lambda^{-1}U^\top$ (pseudo-inverse), we have:

$$A^{-1} b = \sum_{i:\lambda_i > 0} \frac{\beta_i}{\lambda_i} u_i. \tag{43}$$

Also, $(I - \eta A)^s = U(I - \eta\Lambda)^s U^\top$. Therefore:

$$\Delta\theta_s = U\big[I - (I - \eta\Lambda)^s\big]\Lambda^{-1}\beta = \sum_{i:\lambda_i > 0} \frac{1 - (1 - \eta\lambda_i)^s}{\lambda_i} \beta_i u_i. \tag{44}$$

The above expression reveals the directional dynamics. For each eigen-direction u_i, the contribution starts at zero and asymptotically approaches β_i/λ_i. The factor $1 - (1 - \eta\lambda_i)^s$ grows more rapidly when the curvature λ_i is larger, meaning that directions with high sensitivity of the logits to parameter changes saturate early. Consequently, if the projection β_i vanishes for many directions, the effective update remains confined to a low-dimensional subspace throughout training.

A Sufficient Condition for Early Low-Rank Lock-in. Define the top-k eigenspace of A as

$$U_k = \mathrm{span}\{u_1, \ldots, u_k\},$$

and let P_{U_k} be the orthogonal projector onto this subspace. We assume that the driving term b is concentrated in U_k up to a small residual:

$$\|P_{U_k^\perp} b\| \leq \epsilon \|b\|, \qquad \epsilon \ll 1. \tag{45}$$

Equivalently, we decompose

$$b = b_\parallel + b_\perp, \qquad b_\parallel = P_{U_k} b, \qquad b_\perp = P_{U_k^\perp} b.$$

Using the closed-form dynamics, the update can be written as

$$\Delta\theta_s = [I - (I - \eta A)^s] A^{-1} b_\parallel + [I - (I - \eta A)^s] A^{-1} b_\perp. \tag{46}$$

The first term lies in the dominant eigenspace U_k, while the second term corresponds to the tail contribution from $U_k^\perp$. Rather than assuming that A^{-1} is norm-reducing on the orthogonal complement, we bound this tail term through the spectral response of the finite-step dynamics. Specifically,

$$\big\|[I - (I - \eta A)^s] A^{-1} b_\perp\big\| \leq \rho_\perp(s) \|b_\perp\|, \tag{47}$$

where

$$\rho_\perp(s) = \max_{i > k, \lambda_i > 0} \frac{|1 - (1 - \eta\lambda_i)^s|}{\lambda_i}. \tag{48}$$

Combining this with the concentration assumption gives

$$\big\|\Delta\theta_s - [I - (I - \eta A)^s] A^{-1} b_\parallel\big\| \leq \rho_\perp(s) \epsilon \|b\|. \tag{49}$$

Thus, when the projected residual b is highly concentrated in the top-k eigenspace, the tail contribution remains small during the finite training horizon. If, in addition, there is a clear spectral gap,

$$\lambda_k \gg \lambda_{k+1}, \tag{50}$$

then the dominant directions in U_k are activated and saturated earlier than the tail directions. This provides a geometric explanation for **Property 2 (Early Low-Rank Lock-in)**: the optimization path is largely confined to a low-dimensional subspace that is identified in the early stage of training, while subsequent optimization mainly increases the magnitude within this subspace rather than exploring substantially new directions.

Why is b low-rank in practice? Recall that

$$b = \mathbb{E}_c[J_c^\top F_c r_c]. \tag{51}$$

The residual

$$r_c = z^\star(c) - z_0(c)$$

is the teacher-base logit difference. In distillation, the teacher often refines the student by sharpening probabilities on a relatively small set of functionally important token positions, such as key reasoning tokens, intermediate reasoning steps, answer tokens, or formatting tokens (Xu et al., 2026). Hence, r_c is often sparse or low-dimensional in its effective support. The Fisher matrix F_c further reweights these residual directions according to the local geometry of the output distribution. Although J_c itself can be high-rank, the composition

$$J_c^\top F_c r_c$$

projects this concentrated residual signal back into parameter space. After averaging over contexts, the resulting driving term b tends to concentrate on parameter directions that most strongly affect those critical token predictions. This is consistent with the low-rank structure of ΔW observed in Section 3.

Module-Wise Suppression (Functional Redundancy Avoidance). Decompose the parameters into M modules (e.g., embedding, attention, MLP layers). Write:

$$\Delta\theta = (\Delta\theta_1, \Delta\theta_2, \ldots, \Delta\theta_M), \qquad J_c = [J_{c,1}, J_{c,2}, \ldots, J_{c,M}], \tag{52}$$

where $J_{c,m} = \partial z_\theta(c)/\partial\theta_m|_{\theta_0}$. Then the driving term for module m is:

$$b_m = \mathbb{E}_c[J_{c,m}^\top F_c r_c]. \tag{53}$$

The curvature matrix A has block structure:

$$A = \begin{pmatrix} A_{11} & A_{12} & \cdots & A_{1M} \\ A_{21} & A_{22} & \cdots & A_{2M} \\ \vdots & \vdots & \ddots & \vdots \\ A_{M1} & A_{M2} & \cdots & A_{MM} \end{pmatrix}, \quad A_{mn} = \mathbb{E}_c[J_{c,m}^\top F_c J_{c,n}]. \tag{54}$$

At the local optimum $\Delta\theta^* = A^{-1}b$ (or the limit of gradient descent), we have:

$$\sum_{n=1}^{M} A_{mn}\Delta\theta_n^* = b_m. \tag{55}$$

If the cross-module coupling is weak (i.e., A_{mn} is small for $m \neq n$ compared to A_{mm}), and A_{mm} is invertible on its support, then:

$$\Delta\theta_m^* \approx A_{mm}^{-1} b_m. \tag{56}$$

Thus, if $b_m \approx 0$ (module m is weakly coupled with the teacher residual), then $\Delta\theta_m^* \approx 0$. This provides a mechanism for **Property 1 (Functional Redundancy Avoidance)**: modules that do not help match the teacher residual receive negligible updates. Empirically, embedding layers and bottom/top transformer layers have small b_m, leading to suppressed updates.

Comparison with Reinforcement Learning Dynamics. A standard policy gradient update (e.g., PPO) for a trajectory of length T is:

$$g_{\mathrm{RL}} = \mathbb{E}_{x\sim\mathcal{D}, y\sim\pi_\theta(\cdot|x)}\left[\sum_{t=1}^{T} A_t \nabla_\theta \log \pi_\theta(y_t|c_t)\right], \tag{57}$$

where $c_t = (x, y_{<t})$ and A_t is an advantage estimate. Using the logit parameterization:

$$\nabla_\theta \log \pi_\theta(y_t|c_t) = J_{c_t}^\top (e_{y_t} - p_\theta(\cdot|c_t)). \tag{58}$$

Hence:

$$g_{\mathrm{RL}} = \mathbb{E}\left[\sum_{t=1}^{T} A_t J_{c_t}^\top (e_{y_t} - p_\theta(\cdot|c_t))\right]. \tag{59}$$

In contrast, the OPD gradient (local approximation) is:

$$g_{\mathrm{OPD}} = -\nabla_{\Delta\theta}\mathcal{L}_{\mathrm{OPD}} = b - A\Delta\theta. \tag{60}$$

At initialization ($\Delta\theta = 0$), we have $g_{\mathrm{OPD}}(0) = b$, which is a deterministic (up to sampling) function of the teacher residual. The RL gradient at initialization is:

$$g_{\mathrm{RL}}(0) = \mathbb{E}\left[\sum_{t} A_t J_{c_t}^\top (e_{y_t} - p_0(c_t))\right]. \tag{61}$$

The differences between the two paradigms can be summarized in a few key aspects. OPD benefits from dense token-level supervision through the residual r_c (filtered by F_c), whereas RL relies on scalar rewards A_t that are typically zero for most tokens in sparse reward settings, making RL gradient estimates noisier. Moreover, credit assignment in RL is challenging because A_t depends on the entire trajectory and future rewards, introducing high variance. In OPD, the per-token residual provides a more stable learning signal. Finally, the directional structure differs crucially: the OPD driving term b inherits the low-rank concentration of r_c, while the RL driving term involves $e_{y_t} - p_0(c_t)$, a random vector with full support in the vocabulary space, leading to less concentrated and more diffuse updates.

We can approximate the gradient covariance to illustrate the difference. For OPD, the per-sample gradient at initialization is:

$$\hat{g}_{\mathrm{OPD}} = J_c^\top F_c r_c, \tag{62}$$

with covariance $\Sigma_{\mathrm{OPD}} = \mathrm{Cov}(\hat{g}_{\mathrm{OPD}})$. For RL, assuming a single-token simplification (or ignoring temporal dependencies), the per-sample gradient is:

$$\hat{g}_{\mathrm{RL}} = A J_c^\top (e_y - p_0(c)). \tag{63}$$

Its covariance satisfies:

$$\mathrm{Tr}(\Sigma_{\mathrm{RL}}) \approx \mathbb{E}[A^2] \cdot \mathbb{E}[\|J_c^\top (e_y - p_0)\|^2] \;\geq\; \sigma_A^2 \cdot \mathbb{E}[\|J_c^\top (e_y - p_0)\|^2], \tag{64}$$

where $\sigma_A^2 = \mathrm{Var}(A)$. In sparse-reward settings, σ_A^2 can be large because most trajectories receive zero reward except a few. For OPD, the residual r_c is non-zero for many tokens, leading to lower relative variance. Moreover, the norm $\|J_c^\top (e_y - p_0)\|$ is typically larger in magnitude than $\|J_c^\top F_c r_c\|$ when r_c is small, because F_c has eigenvalues at most 1. Consequently, we expect $\mathrm{Tr}(\Sigma_{\mathrm{RL}}) > \mathrm{Tr}(\Sigma_{\mathrm{OPD}})$ in practice, implying that OPD follows a smoother and lower-noise optimization trajectory.

Summary. In the local regime, OPD can be approximated by a possibly degenerate convex quadratic minimization:

$$\min_{\Delta\theta} \frac{1}{2}\Delta\theta^\top A \Delta\theta - b^\top \Delta\theta. \tag{65}$$

The corresponding gradient descent dynamics admit the spectral form:

$$\Delta\theta_s = \sum_{i:\lambda_i>0} \frac{1-(1-\eta\lambda_i)^s}{\lambda_i}\beta_i u_i. \tag{66}$$

This expression shows that the update along each eigen-direction is determined by the residual projection $\beta_i = \langle b, u_i \rangle$, the local curvature λ_i, and the finite-step growth factor $1 - (1 - \eta\lambda_i)^s$.

If the driving term b is concentrated in a low-dimensional subspace, such as the top-k eigenspace of A, and a clear spectral gap exists, then the update remains approximately confined to this subspace from the early stages of training. This provides a local explanation for **Early Low-Rank Lock-in**. At the module level, if a module has negligible coupling with the teacher residual, i.e., $b_m \approx 0$, then its update is expected to be suppressed when cross-module coupling terms are not dominant. This explains **Functional Redundancy Avoidance**. Compared with RL, OPD benefits from a denser, lower-variance, and more directionally concentrated gradient signal, which helps explain the more concentrated and efficient update patterns observed in OPD.

Question

Let $\triangle ABC$ be a triangle with D on $\overline{BC}$ such that $\overline{AD}$ bisects $\angle BAC$. Let ω be the circle that passes through A and is tangent to segment $\overline{BC}$ at D. Let $E \neq A$ and $F \neq A$ be the intersections of ω with segments $\overline{AB}$ and $\overline{AC}$, respectively. Suppose that $AB = 200, AC = 225$, and all of AE, AF, BD, and CD are positive integers. Find the sum of all possible values of BC.

Base Model

We are given that Patrick, Tanya, and Jose start at different times and all arrive at the park at the same time. We need to find the distance $D = \dfrac{m}{n}$ in lowest terms, then compute $m + n$.

Step 1: Define Variables.
Let v be Patrick's speed (mph). Then Tanya's speed is $v + 2$ and Jose's speed is $v + 9$. Let t be Patrick's travel time (hours). Since they all arrive simultaneously, Tanya travels $t - 1$ hours and Jose travels $t - 2$ hours, giving:

$$D = vt = (v + 2)(t - 1) = (v + 9)(t - 2).$$

Step 2: Solve for t and v.
From $vt = (v + 2)(t - 1)$:

$$vt = vt - v + 2t - 2 \implies v = 2t - 2. \tag{A}$$

From $(v + 2)(t - 1) = (v + 9)(t - 2)$:

$$vt - v + 2t - 2 = vt - 2v + 9t - 18 \implies v = 7t - 16. \tag{B}$$

Setting (A) equal to (B):

$$2t - 2 = 7t - 16 \implies 5t = 14 \implies t = \frac{14}{5}.$$

Substituting back into (A):

$$v = 2 \cdot \frac{14}{5} - 2 = \frac{28}{5} - \frac{10}{5} = \frac{18}{5} \text{ mph}.$$

Step 3: Compute the Distance.

$$D = vt = \frac{18}{5} \times \frac{14}{5} = \frac{252}{25}.$$

Since $252 = 2^2 \times 3^2 \times 7$ and $25 = 5^2$ share no common factors, $\gcd(252, 25) = 1$, so the fraction is already in lowest terms.

Final Answer.

$$m + n = 252 + 25 = \boxed{277}.$$

The early training stage model (unscaled)

We are given that Patrick starts walking at a constant rate, Tanya starts 1 hour after Patrick, and Jose starts 1 hour after Tanya. All three arrive at the park at the same time. Tanya runs 2 mph faster than Patrick walks, and Jose bicycles 7 mph faster than Tanya runs. The distance from school to park is $\frac{m}{n}$ in lowest terms; find $m + n$.

Step 1: Define Variables.
Let p be Patrick's walking speed (mph), so Tanya's running speed is $p+2$ and Jose's bicycling speed is $p + 9$. Let D be the distance (miles) and T the total travel time (hours) for Patrick.

Step 2: Set Up Equations.

Since all three arrive simultaneously:

$$D = p \cdot T, \tag{1}$$
$$D = (p+2)(T-1), \tag{2}$$
$$D = (p+9)(T-2). \tag{3}$$

Step 3: Solve for p and T.
Equating (1) and (2):

$$pT = (p+2)(T-1) = pT - p + 2T - 2 \implies p = 2T - 2. \tag{4}$$

Equating (2) and (3):

$$(p+2)(T-1) = (p+9)(T-2).$$

Expanding both sides and simplifying:

$$-p + 2T - 2 = -2p + 9T - 18 \implies p = 7T - 16. \tag{5}$$

Setting (4) equal to (5):

$$2T - 2 = 7T - 16 \implies 5T = 14 \implies T = \frac{14}{5}.$$

Substituting back into (4):

$$p = 2 \cdot \frac{14}{5} - 2 = \frac{18}{5} \text{ mph.}$$

Step 4: Compute the Distance.

$$D = pT = \frac{18}{5} \cdot \frac{14}{5} = \frac{252}{25}.$$

Since $252 = 2^2 \cdot 3^2 \cdot 7$ and $25 = 5^2$ share no common factors, $\gcd(252, 25) = 1$.

Verification.

$$p = \frac{18}{5}, \quad p+2 = \frac{28}{5}, \quad p+9 = \frac{63}{5},$$
$$D = \frac{18}{5} \cdot \frac{14}{5} = \frac{252}{25}, \quad \frac{252/25}{28/5} = \frac{252}{25} \cdot \frac{5}{28} = \frac{9}{5} = T-1\,, \quad \frac{252/25}{63/5} = \frac{252}{25} \cdot \frac{5}{63} = \frac{4}{5} = T-2\,.$$

Answer.

$$m + n = 252 + 25 = \boxed{277}.$$

The early training stage model (scaled):

We are given a problem involving three people—Patrick, Tanya, and Jose—each starting at different times and moving along the same path from school to the park. All three arrive at the park at the same time. We need to find the distance from school to park, expressed as a reduced fraction $\frac{m}{n}$, and then compute $m + n$. **Step 1: Define Variables.**

Let v be Patrick's walking speed (in miles per hour). Then:

- Tanya's running speed is $v + 2$ mph (2 mph faster than Patrick),
- Jose's bicycling speed is $(v + 2) + 7 = v + 9$ mph (7 mph faster than Tanya).

Let D be the distance from school to park (in miles), and let t be the time (in hours) that Patrick takes to walk from school to park. Since all three arrive at the same time:

- Patrick travels for t hours,
- Tanya starts 1 hour after Patrick, so she travels for $t - 1$ hours,

- Jose starts 1 hour after Tanya (2 hours after Patrick), so he travels for $t-2$ hours.

This gives the following time equations:

$$t = \frac{D}{v}, \qquad \frac{D}{v+2} = t-1, \qquad \frac{D}{v+9} = t-2.$$

Step 2: Substitute $t = D/v$ into the Remaining Equations.

Substituting $t = \dfrac{D}{v}$ into the equation for Tanya:

$$\frac{D}{v+2} = \frac{D}{v} - 1.$$

Substituting $t = \dfrac{D}{v}$ into the equation for Jose:

$$\frac{D}{v+9} = \frac{D}{v} - 2.$$

We now have two equations in two unknowns D and v.

Step 3: Derive Equation (A) from Tanya's Equation.

Starting from:

$$\frac{D}{v+2} = \frac{D}{v} - 1.$$

Multiply both sides by $v(v+2)$:

$$D \cdot v = D(v+2) - v(v+2).$$

Expand the right-hand side:

$$Dv = Dv + 2D - v^2 - 2v.$$

Subtract Dv from both sides:

$$0 = 2D - v^2 - 2v.$$

Rearranging:

$$v^2 + 2v - 2D = 0. \tag{A}$$

Step 4: Derive Equation (B) from Jose's Equation.

Starting from:

$$\frac{D}{v+9} = \frac{D}{v} - 2.$$

Multiply both sides by $v(v+9)$:

$$D \cdot v = D(v+9) - 2v(v+9).$$

Expand the right-hand side:

$$Dv = Dv + 9D - 2v^2 - 18v.$$

Subtract Dv from both sides:

$$0 = 9D - 2v^2 - 18v.$$

Rearranging:

$$2v^2 + 18v - 9D = 0. \tag{B}$$

Step 5: Solve the System of Equations (A) and (B).

From equation (A):

$$v^2 + 2v - 2D = 0 \implies D = \frac{v^2 + 2v}{2}.$$

Substitute this expression for D into equation (B):

$$2v^2 + 18v - 9 \cdot \frac{v^2 + 2v}{2} = 0.$$

Multiply every term by 2 to clear the denominator:

$$4v^2 + 36v - 9(v^2 + 2v) = 0.$$

Expand:

$$4v^2 + 36v - 9v^2 - 18v = 0.$$

Combine like terms:

$$(4v^2 - 9v^2) + (36v - 18v) = 0 \implies -5v^2 + 18v = 0.$$

Factor:

$$v(-5v + 18) = 0.$$

This gives $v = 0$ or $v = \frac{18}{5}$. Since Patrick is walking, $v > 0$, so:

$$v = \frac{18}{5} \text{ mph.}$$

Step 6: Compute the Distance D.
Using $D = \frac{v^2 + 2v}{2}$ with $v = \frac{18}{5}$:

$$v^2 = \left(\frac{18}{5}\right)^2 = \frac{324}{25}, \qquad 2v = 2 \times \frac{18}{5} = \frac{36}{5} = \frac{180}{25}.$$

$$v^2 + 2v = \frac{324}{25} + \frac{180}{25} = \frac{504}{25}.$$

$$D = \frac{504/25}{2} = \frac{504}{50} = \frac{252}{25}.$$

Step 7: Verify with All Three Travelers.
Patrick's travel time: $t = \frac{D}{v} = \frac{252/25}{18/5} = \frac{252}{25} \times \frac{5}{18} = \frac{1260}{450} = \frac{14}{5}$ hours.

Tanya travels for $t - 1 = \frac{14}{5} - \frac{5}{5} = \frac{9}{5}$ hours at speed $v + 2 = \frac{18}{5} + \frac{10}{5} = \frac{28}{5}$ mph:

$$\frac{28}{5} \times \frac{9}{5} = \frac{252}{25} = D. \quad \checkmark$$

Jose travels for $t - 2 = \frac{14}{5} - \frac{10}{5} = \frac{4}{5}$ hours at speed $v + 9 = \frac{18}{5} + \frac{45}{5} = \frac{63}{5}$ mph:

$$\frac{63}{5} \times \frac{4}{5} = \frac{252}{25} = D. \quad \checkmark$$

All three cover the same distance and arrive at the same time.

Step 8: Confirm the Fraction is in Lowest Terms.
Factoring numerator and denominator:

$$252 = 2^2 \times 3^2 \times 7, \qquad 25 = 5^2.$$

Since 252 contains no factor of 5 (as $252 \div 5 = 50.4$ is not an integer) and 25 contains no factor of 2, 3, or 7, we have $\gcd(252, 25) = 1$. Therefore $\frac{252}{25}$ is already in lowest terms, giving $m = 252$ and $n = 25$.

Final Answer.

$$m + n = 252 + 25 = \boxed{277}.$$

Teacher Model

We are given a problem involving three people—Patrick, Tanya, and Jose—each starting at different times and moving along the same road from school to the park. They all arrive at the park at the same time. We need to find the distance from school to park, expressed as a reduced fraction $\frac{m}{n}$, and then compute $m+n$.

Step 1: Define Variables.
Let d be the distance from school to park (in miles) and v be Patrick's walking speed (in mph). Then:

- Tanya's running speed is $v+2$ mph (2 mph faster than Patrick),
- Jose's bicycling speed is $(v+2)+7 = v+9$ mph (7 mph faster than Tanya).

Step 2: Determine Travel Times.
Let t be the number of hours Patrick takes to reach the park. Since Tanya starts 1 hour after Patrick and arrives at the same time, she travels for $t-1$ hours. Since Jose starts 1 hour after Tanya (i.e., 2 hours after Patrick) and arrives at the same time, he travels for $t-2$ hours.
Using distance $=$ speed $\times$ time, we obtain three equations:

$$v = \frac{d}{t}, \tag{1}$$

$$v+2 = \frac{d}{t-1}, \tag{2}$$

$$v+9 = \frac{d}{t-2}. \tag{3}$$

Step 3: Derive Equation (A) from Equations (1) and (2).
From equation (1): $t = \frac{d}{v}$. Substituting into equation (2):

$$v+2 = \frac{d}{\frac{d}{v}-1} = \frac{d}{\frac{d-v}{v}} = \frac{dv}{d-v}.$$

Multiply both sides by $(d-v)$:

$$(v+2)(d-v) = dv.$$

Expand the left-hand side:

$$vd - v^2 + 2d - 2v = dv.$$

Subtract dv from both sides:

$$-v^2 + 2d - 2v = 0.$$

Rearranging:

$$v^2 + 2v - 2d = 0. \tag{A}$$

Step 4: Derive Equation (B) from Equations (1) and (3).
Again using $t = \frac{d}{v}$, we have $t-2 = \frac{d}{v} - 2 = \frac{d-2v}{v}$. Substituting into equation (3):

$$v+9 = \frac{d}{\frac{d-2v}{v}} = \frac{dv}{d-2v}.$$

Multiply both sides by $(d-2v)$:

$$(v+9)(d-2v) = dv.$$

Expand the left-hand side:

$$vd - 2v^2 + 9d - 18v = dv.$$

Subtract dv from both sides:

$$-2v^2 + 9d - 18v = 0.$$

Rearranging:

$$2v^2 + 18v - 9d = 0. \tag{B}$$

Step 5: Solve the System of Equations (A) and (B).
From equation (A):

$$2d = v^2 + 2v \implies d = \frac{v^2 + 2v}{2}.$$

Substitute this expression for d into equation (B):

$$2v^2 + 18v - 9 \cdot \frac{v^2 + 2v}{2} = 0.$$

Multiply every term by 2 to clear the denominator:

$$4v^2 + 36v - 9(v^2 + 2v) = 0.$$

Expand:

$$4v^2 + 36v - 9v^2 - 18v = 0.$$

Combine like terms:

$$(4v^2 - 9v^2) + (36v - 18v) = 0 \implies -5v^2 + 18v = 0.$$

Factor:

$$v(-5v + 18) = 0.$$

This gives $v = 0$ or $v = \frac{18}{5}$. Since Patrick is walking, $v > 0$, so:

$$v = \frac{18}{5} \text{ mph.}$$

Step 6: Compute the Speeds.

- Patrick's speed: $v = \frac{18}{5}$ mph,
- Tanya's speed: $v + 2 = \frac{18}{5} + \frac{10}{5} = \frac{28}{5}$ mph,
- Jose's speed: $v + 9 = \frac{18}{5} + \frac{45}{5} = \frac{63}{5}$ mph.

Step 7: Compute the Distance d.

$$d = \frac{v^2 + 2v}{2}.$$

First compute v^2:

$$v^2 = \left(\frac{18}{5}\right)^2 = \frac{324}{25}.$$

Then compute $2v$:

$$2v = 2 \times \frac{18}{5} = \frac{36}{5} = \frac{180}{25}.$$

Add:

$$v^2 + 2v = \frac{324}{25} + \frac{180}{25} = \frac{504}{25}.$$

Divide by 2:

$$d = \frac{504}{25} \div 2 = \frac{504}{50} = \frac{252}{25}.$$

Step 8: Verify the Answer.

Patrick's total travel time:

$$t = \frac{d}{v} = \frac{252/25}{18/5} = \frac{252}{25} \times \frac{5}{18} = \frac{252 \times 5}{25 \times 18} = \frac{1260}{450} = \frac{14}{5} \text{ hours.}$$

Tanya travels for $t - 1 = \frac{14}{5} - \frac{5}{5} = \frac{9}{5}$ hours at speed $\frac{28}{5}$ mph:

$$\frac{28}{5} \times \frac{9}{5} = \frac{252}{25} \checkmark.$$

Jose travels for $t - 2 = \frac{14}{5} - \frac{10}{5} = \frac{4}{5}$ hours at speed $\frac{63}{5}$ mph:

$$\frac{63}{5} \times \frac{4}{5} = \frac{252}{25} \checkmark.$$

All three cover the same distance $\frac{252}{25}$ miles.

Step 9: Confirm the Fraction is in Lowest Terms.
Factoring the numerator and denominator:

$$252 = 2^2 \times 3^2 \times 7, \qquad 25 = 5^2.$$

Since 252 and 25 share no common prime factors, $\gcd(252, 25) = 1$, so $\frac{252}{25}$ is already in lowest terms.

Final Answer.

$$m + n = 252 + 25 = \boxed{277}.$$

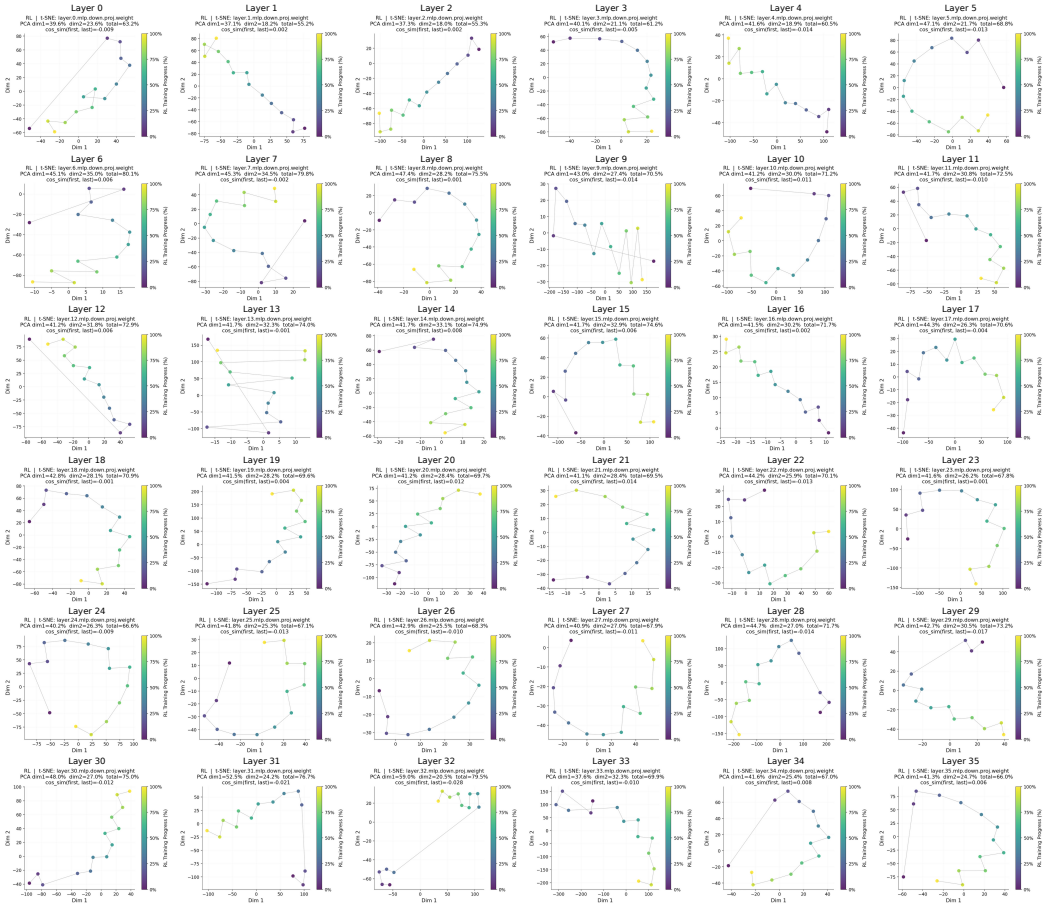

Figure 15: t-SNE visualization of $\mathcal{U}_1$ trajectories under DAPO for MLP modules.

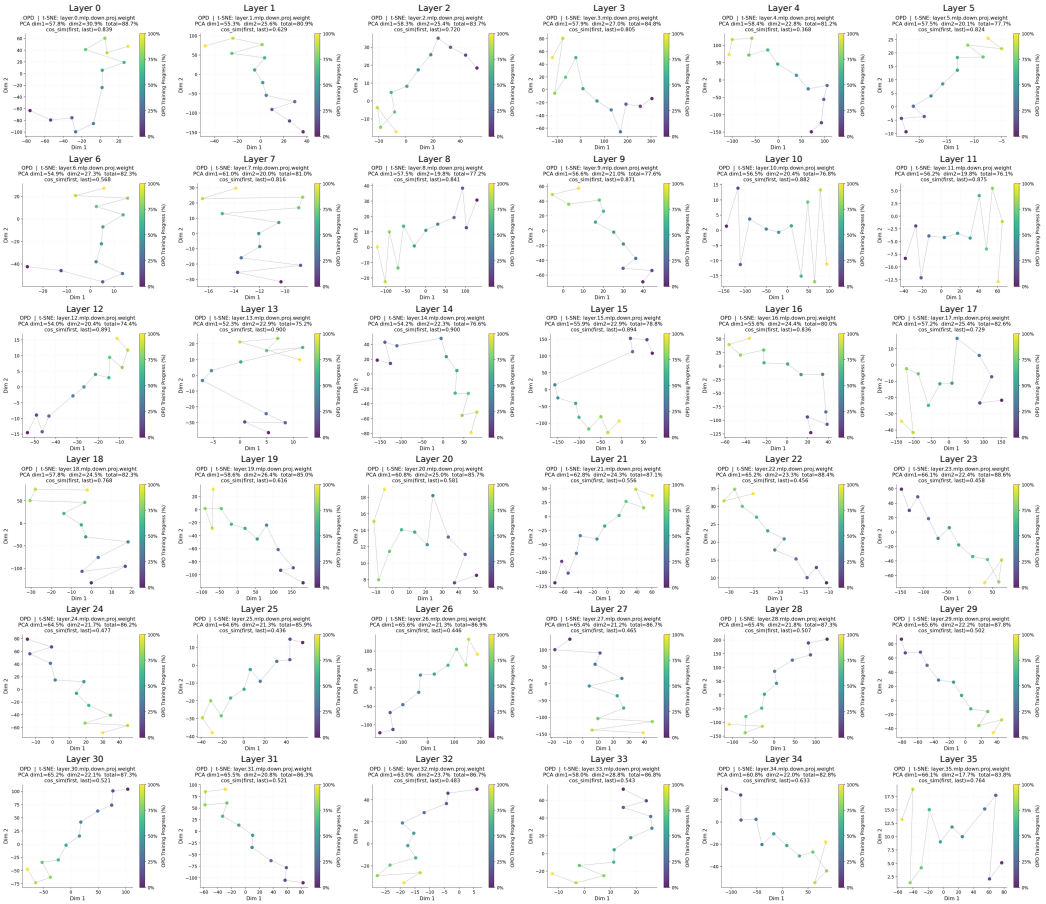

Figure 16: t-SNE visualization of $\mathcal{U}_1$ trajectories under OPD for MLP modules.

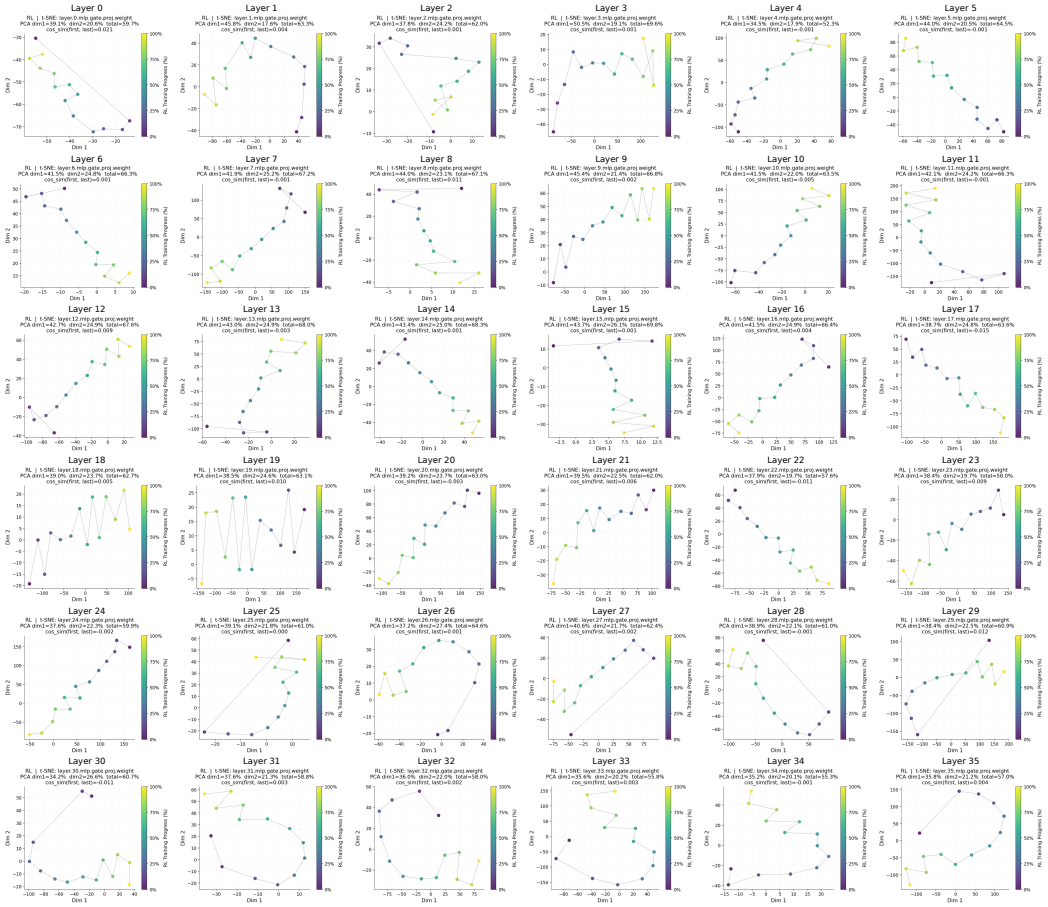

Figure 17: t-SNE visualization of $\mathcal{U}_1$ trajectories under DAPO for MLP GATE modules.

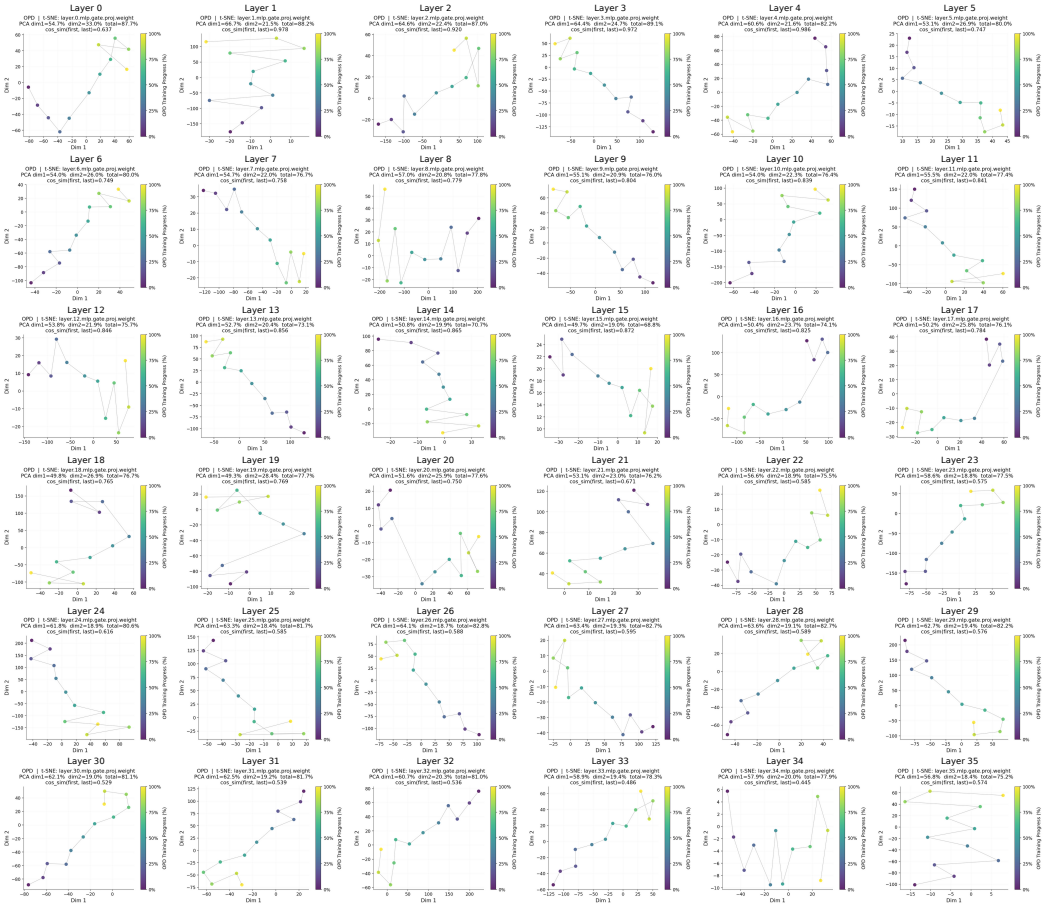

Figure 18: t-SNE visualization of $\mathcal{U}_1$ trajectories under OPD for MLP GATE modules.

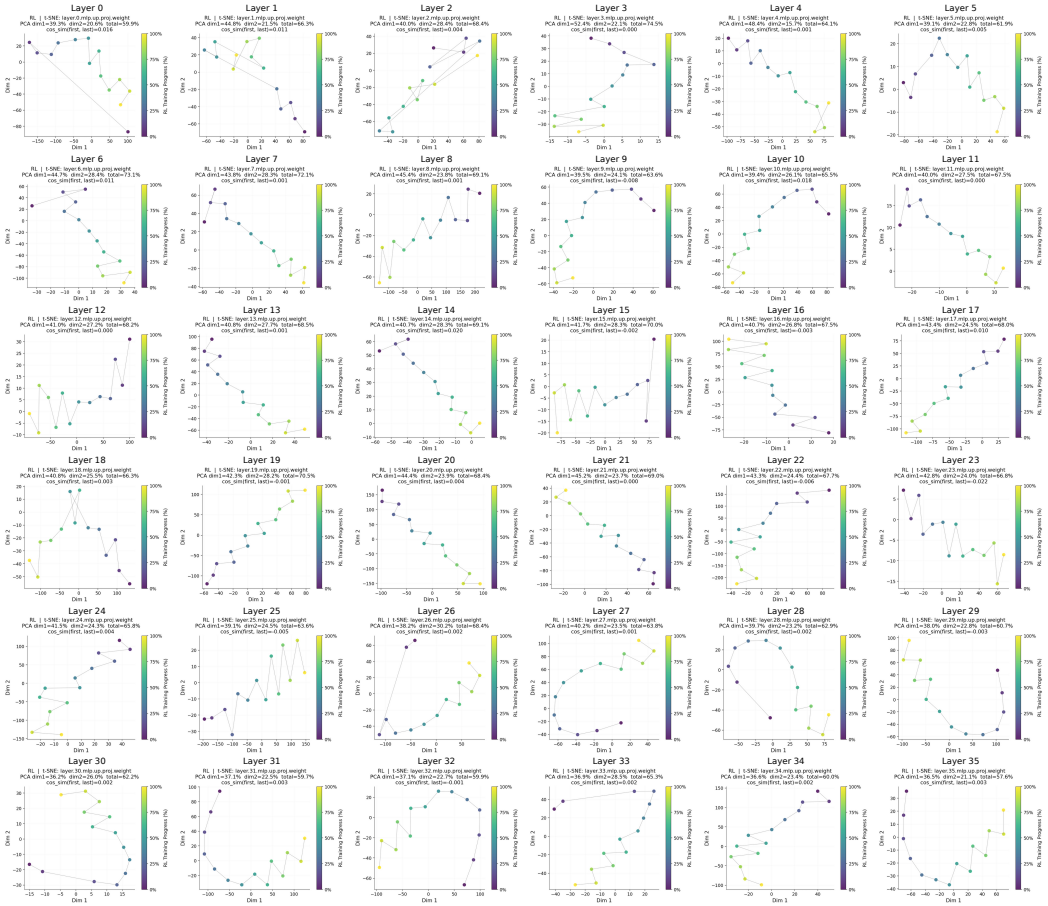

Figure 19: t-SNE visualization of $\mathcal{U}_1$ trajectories under DAPO for MLP UP modules.

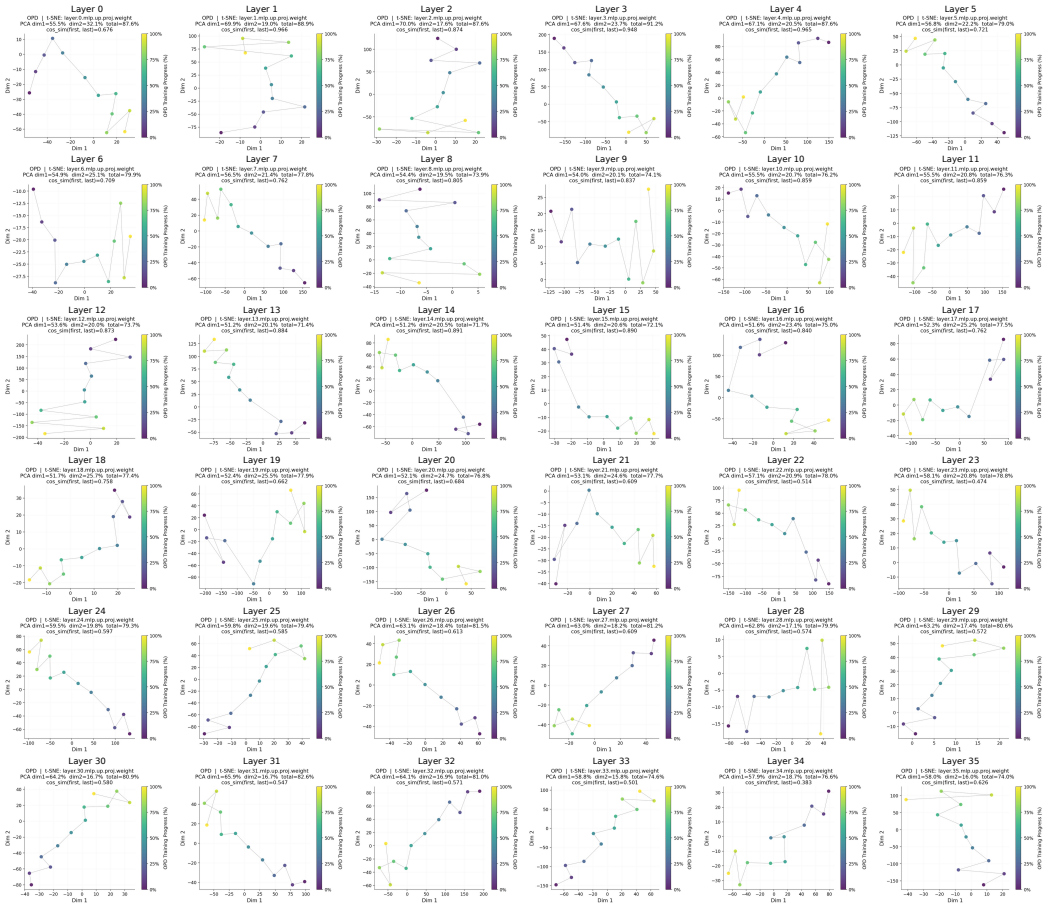

Figure 20: t-SNE visualization of $\mathcal{U}_1$ trajectories under OPD for MLP UP modules.

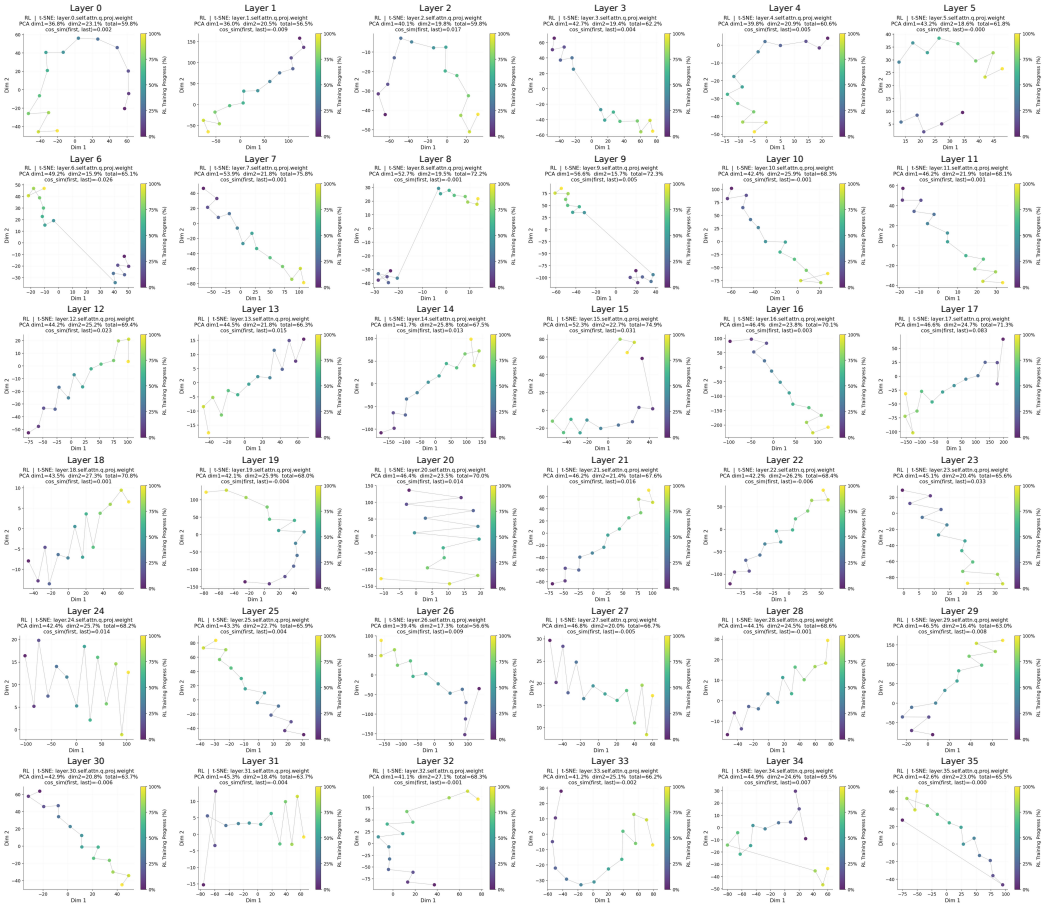

Figure 21: t-SNE visualization of $\mathcal{U}_1$ trajectories under DAPO for Attn Q modules.

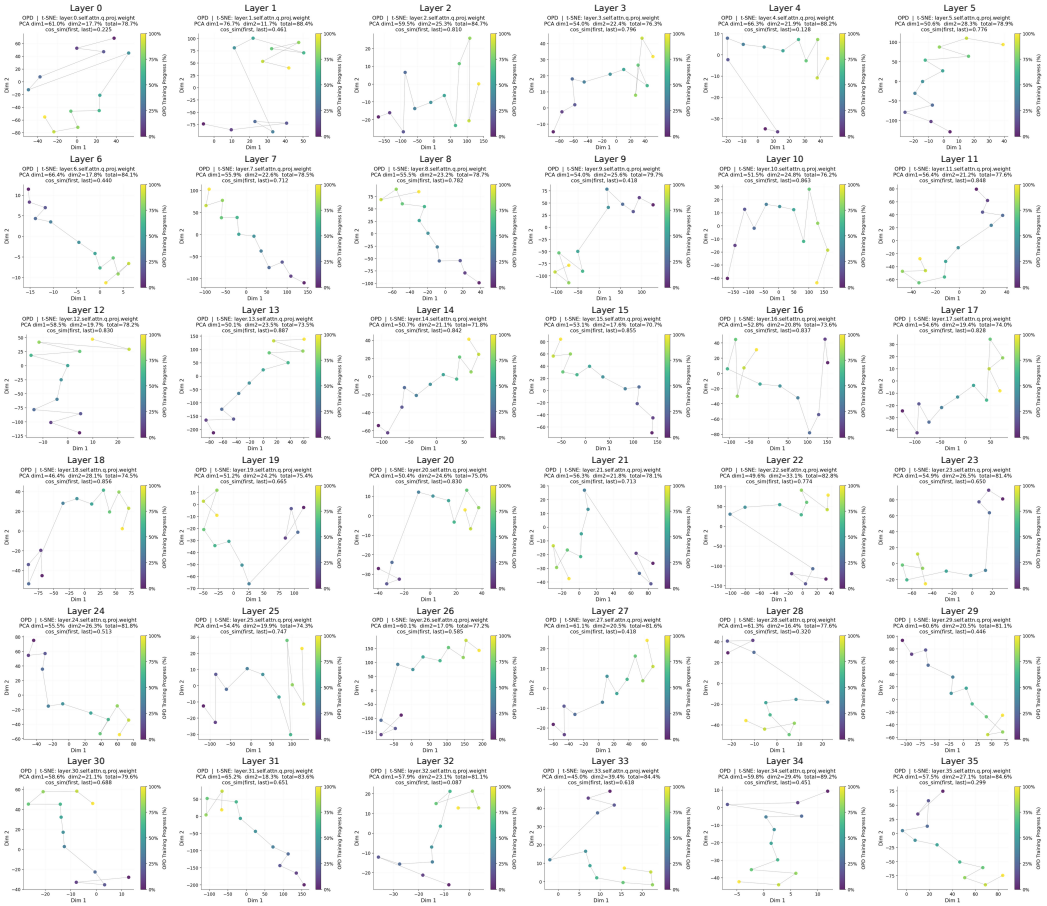

Figure 22: t-SNE visualization of $\mathcal{U}_1$ trajectories under OPD for Attn Q modules.

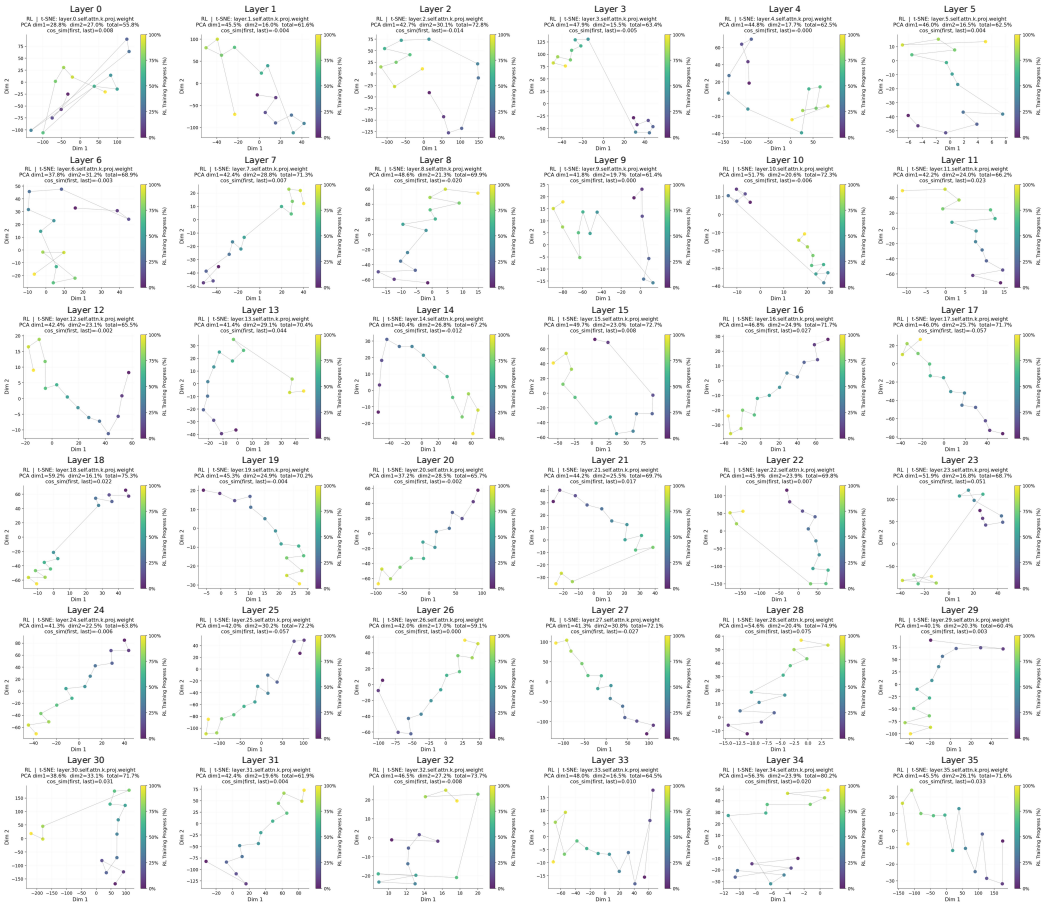

Figure 23: t-SNE visualization of $\mathcal{U}_1$ trajectories under DAPO for Attn K modules.

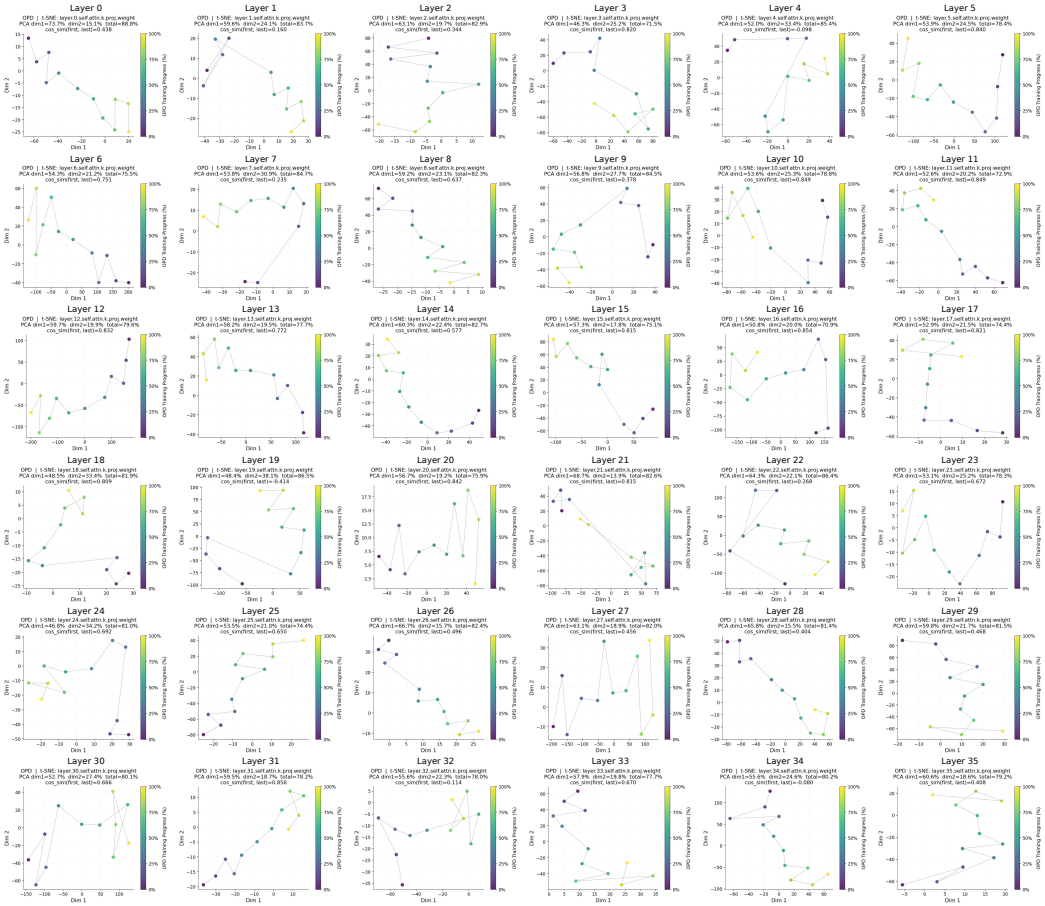

Figure 24: t-SNE visualization of $\mathcal{U}_1$ trajectories under OPD for Attn K modules.

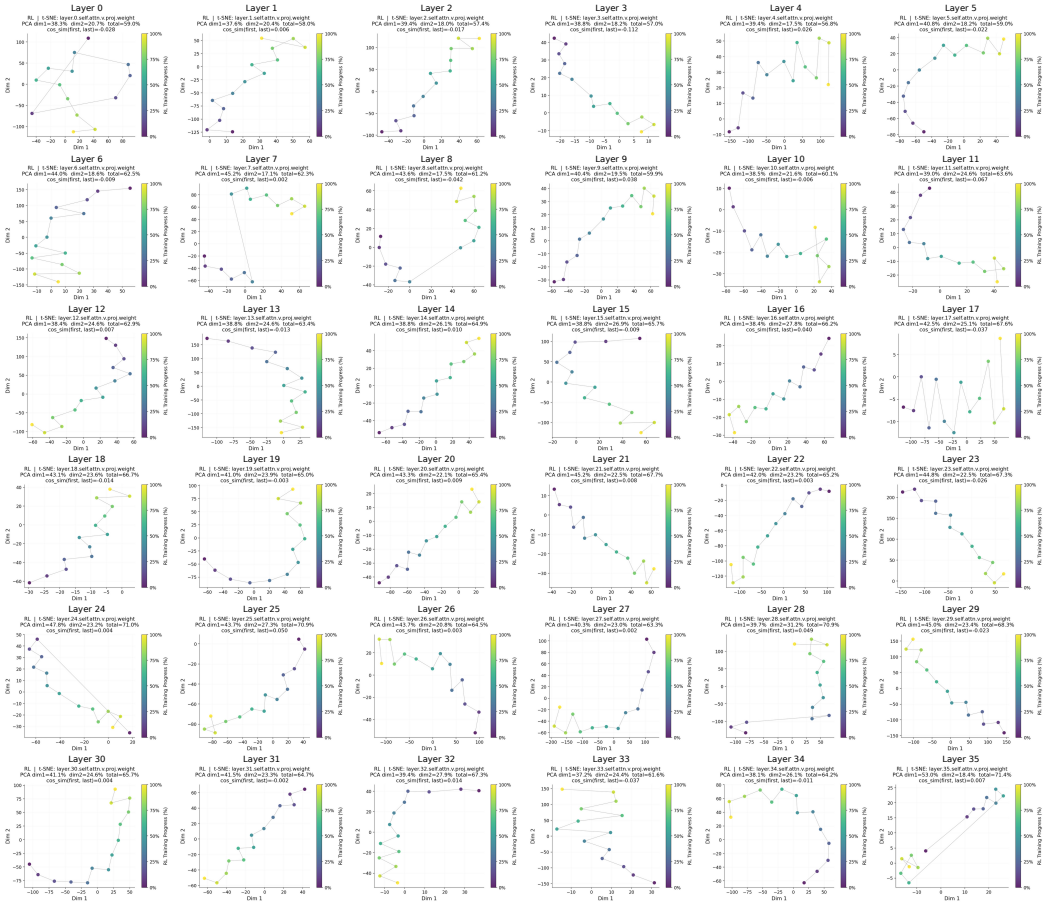

Figure 25: t-SNE visualization of $\mathcal{U}_1$ trajectories under DAPO for Attn V modules.

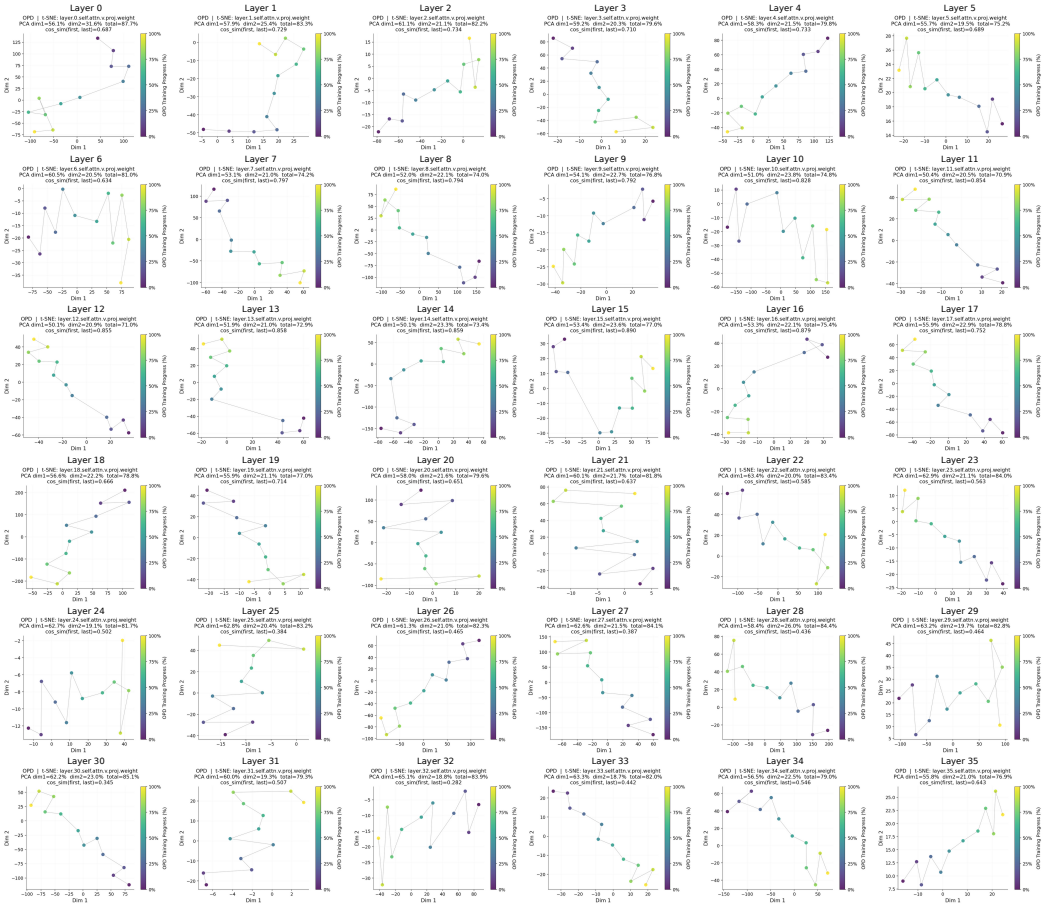

Figure 26: t-SNE visualization of $\mathcal{U}_1$ trajectories under OPD for Attn V modules.

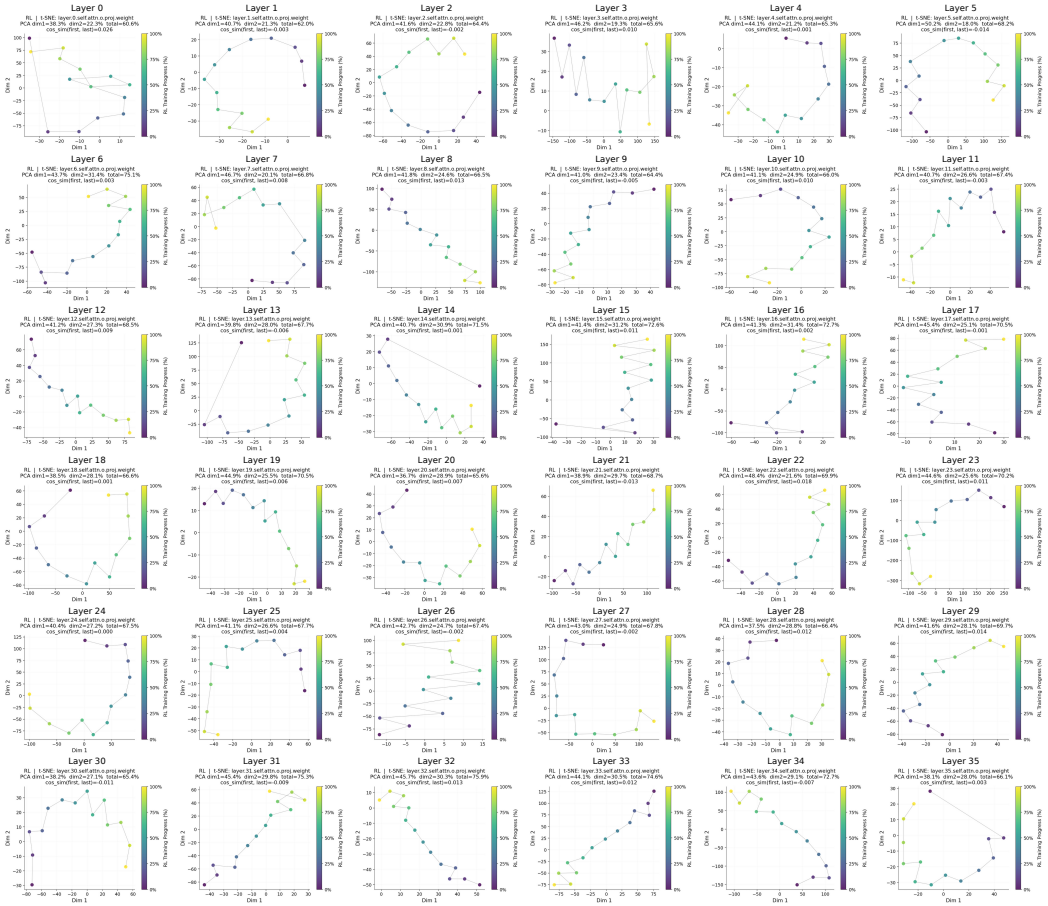

Figure 27: t-SNE visualization of $\mathcal{U}_1$ trajectories under DAPO for Attn modules.

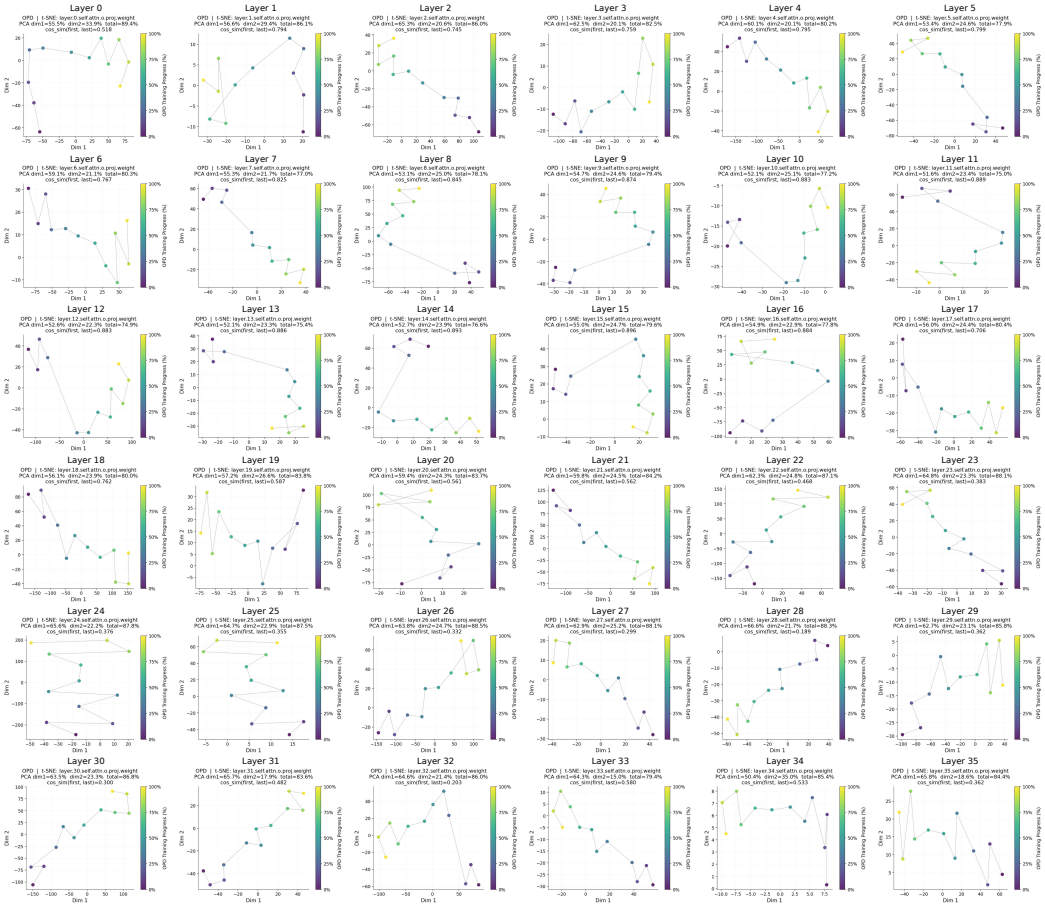

Figure 28: t-SNE visualization of $\mathcal{U}_1$ trajectories under OPD for Attn modules.

G NeurIPS Paper Checklist

1. **Claims**

   Answer: [Yes]

   Justification: The abstract and introduction clearly state the paper's main contributions: identifying the foresight mechanism of OPD through Functional Redundancy Avoidance and Early Low-Rank Lock-in, and proposing EffOPD as a plug-and-play acceleration method.

   Guidelines:

   - The answer [N/A] means that the abstract and introduction do not include the claims made in the paper.
   - The abstract and/or introduction should clearly state the claims made, including the contributions made in the paper and important assumptions and limitations. A [No] or [N/A] answer to this question will not be perceived well by the reviewers.
   - The claims made should match theoretical and experimental results, and reflect how much the results can be expected to generalize to other settings.
   - It is fine to include aspirational goals as motivation as long as it is clear that these goals are not attained by the paper.

2. **Limitations**

   Answer: [Yes]

   Justification: The paper includes a Limitations and Future Work section discussing the scope of the analysis, including its focus on current post-training settings and the local nature of the theoretical analysis.

   Guidelines:

   - The answer [N/A] means that the paper has no limitation while the answer [No] means that the paper has limitations, but those are not discussed in the paper.
   - The authors are encouraged to create a separate "Limitations" section in their paper.
   - The paper should point out any strong assumptions and how robust the results are to violations of these assumptions (e.g., independence assumptions, noiseless settings, model well-specification, asymptotic approximations only holding locally). The authors should reflect on how these assumptions might be violated in practice and what the implications would be.
   - The authors should reflect on the scope of the claims made, e.g., if the approach was only tested on a few datasets or with a few runs. In general, empirical results often depend on implicit assumptions, which should be articulated.
   - The authors should reflect on the factors that influence the performance of the approach. For example, a facial recognition algorithm may perform poorly when image resolution is low or images are taken in low lighting. Or a speech-to-text system might not be used reliably to provide closed captions for online lectures because it fails to handle technical jargon.
   - The authors should discuss the computational efficiency of the proposed algorithms and how they scale with dataset size.
   - If applicable, the authors should discuss possible limitations of their approach to address problems of privacy and fairness.
   - While the authors might fear that complete honesty about limitations might be used by reviewers as grounds for rejection, a worse outcome might be that reviewers discover limitations that aren't acknowledged in the paper. The authors should use their best judgment and recognize that individual actions in favor of transparency play an important role in developing norms that preserve the integrity of the community. Reviewers will be specifically instructed to not penalize honesty concerning limitations.

3. **Theory assumptions and proofs**

   Answer: [Yes]

   Justification: The paper provides theoretical analysis in the appendix, including the assumptions behind the local linearization of OPD dynamics.

Guidelines:

- The answer [N/A] means that the paper does not include theoretical results.
- All the theorems, formulas, and proofs in the paper should be numbered and cross-referenced.
- All assumptions should be clearly stated or referenced in the statement of any theorems.
- The proofs can either appear in the main paper or the supplemental material, but if they appear in the supplemental material, the authors are encouraged to provide a short proof sketch to provide intuition.
- Inversely, any informal proof provided in the core of the paper should be complemented by formal proofs provided in appendix or supplemental material.
- Theorems and Lemmas that the proof relies upon should be properly referenced.

4. **Experimental result reproducibility**

   Answer: [Yes]

   Justification: The paper describes the training datasets, model scales, teacher models, evaluation benchmarks, baselines, and the EffOPD procedure needed to reproduce the main experimental results.

   Guidelines:

   - The answer [N/A] means that the paper does not include experiments.
   - If the paper includes experiments, a [No] answer to this question will not be perceived well by the reviewers: Making the paper reproducible is important, regardless of whether the code and data are provided or not.
   - If the contribution is a dataset and/or model, the authors should describe the steps taken to make their results reproducible or verifiable.
   - Depending on the contribution, reproducibility can be accomplished in various ways. For example, if the contribution is a novel architecture, describing the architecture fully might suffice, or if the contribution is a specific model and empirical evaluation, it may be necessary to either make it possible for others to replicate the model with the same dataset, or provide access to the model. In general. releasing code and data is often one good way to accomplish this, but reproducibility can also be provided via detailed instructions for how to replicate the results, access to a hosted model (e.g., in the case of a large language model), releasing of a model checkpoint, or other means that are appropriate to the research performed.
   - While NeurIPS does not require releasing code, the conference does require all submissions to provide some reasonable avenue for reproducibility, which may depend on the nature of the contribution. For example
     (a) If the contribution is primarily a new algorithm, the paper should make it clear how to reproduce that algorithm.
     (b) If the contribution is primarily a new model architecture, the paper should describe the architecture clearly and fully.
     (c) If the contribution is a new model (e.g., a large language model), then there should either be a way to access this model for reproducing the results or a way to reproduce the model (e.g., with an open-source dataset or instructions for how to construct the dataset).
     (d) We recognize that reproducibility may be tricky in some cases, in which case authors are welcome to describe the particular way they provide for reproducibility. In the case of closed-source models, it may be that access to the model is limited in some way (e.g., to registered users), but it should be possible for other researchers to have some path to reproducing or verifying the results.

5. **Open access to data and code**

   Answer: [Yes]

   Justification: The paper uses publicly available datasets and models. This paper releases the code used in this work through an anonymous link: https://anonymous.4open.science/r/EffOPD-7C58.

   Guidelines:

- The answer [N/A] means that paper does not include experiments requiring code.
- Please see the NeurIPS code and data submission guidelines (https://neurips.cc/public/guides/CodeSubmissionPolicy) for more details.
- While we encourage the release of code and data, we understand that this might not be possible, so [No] is an acceptable answer. Papers cannot be rejected simply for not including code, unless this is central to the contribution (e.g., for a new open-source benchmark).
- The instructions should contain the exact command and environment needed to run to reproduce the results. See the NeurIPS code and data submission guidelines (https://neurips.cc/public/guides/CodeSubmissionPolicy) for more details.
- The authors should provide instructions on data access and preparation, including how to access the raw data, preprocessed data, intermediate data, and generated data, etc.
- The authors should provide scripts to reproduce all experimental results for the new proposed method and baselines. If only a subset of experiments are reproducible, they should state which ones are omitted from the script and why.
- At submission time, to preserve anonymity, the authors should release anonymized versions (if applicable).
- Providing as much information as possible in supplemental material (appended to the paper) is recommended, but including URLs to data and code is permitted.

6. **Experimental setting/details**

   Answer: [Yes]

   Justification: The paper specifies the training tasks, datasets, model scales, teacher models, baselines, evaluation benchmarks, sampling settings, and key hyperparameters of EffOPD.

   Guidelines:

   - The answer [N/A] means that the paper does not include experiments.
   - The experimental setting should be presented in the core of the paper to a level of detail that is necessary to appreciate the results and make sense of them.
   - The full details can be provided either with the code, in appendix, or as supplemental material.

7. **Experiment statistical significance**

   Answer: [No]

   Justification: The paper reports performance trends across model scales, datasets, and baselines, but does not include formal error bars or statistical significance tests for all experiments.

   Guidelines:

   - The answer [N/A] means that the paper does not include experiments.
   - The authors should answer [Yes] if the results are accompanied by error bars, confidence intervals, or statistical significance tests, at least for the experiments that support the main claims of the paper.
   - The factors of variability that the error bars are capturing should be clearly stated (for example, train/test split, initialization, random drawing of some parameter, or overall run with given experimental conditions).
   - The method for calculating the error bars should be explained (closed form formula, call to a library function, bootstrap, etc.)
   - The assumptions made should be given (e.g., Normally distributed errors).
   - It should be clear whether the error bar is the standard deviation or the standard error of the mean.
   - It is OK to report 1-sigma error bars, but one should state it. The authors should preferably report a 2-sigma error bar than state that they have a 96% CI, if the hypothesis of Normality of errors is not verified.
   - For asymmetric distributions, the authors should be careful not to show in tables or figures symmetric error bars that would yield results that are out of range (e.g., negative error rates).

- If error bars are reported in tables or plots, the authors should explain in the text how they were calculated and reference the corresponding figures or tables in the text.

8. **Experiments compute resources**

   Answer: [No]

   Justification: The paper discusses the computational overhead of EffOPD, but does not yet provide full details of the hardware configuration, memory usage, or total compute required for each experiment.

   - The answer [N/A] means that the paper does not include experiments.
   - The paper should indicate the type of compute workers CPU or GPU, internal cluster, or cloud provider, including relevant memory and storage.
   - The paper should provide the amount of compute required for each of the individual experimental runs as well as estimate the total compute.
   - The paper should disclose whether the full research project required more compute than the experiments reported in the paper (e.g., preliminary or failed experiments that didn't make it into the paper).

9. **Code of ethics**

   Answer: [Yes]

   Justification: We have reviewed the NeurIPS Code of Ethics and believe the research conforms to it.

   Guidelines:

   - The answer [N/A] means that the authors have not reviewed the NeurIPS Code of Ethics.
   - If the authors answer [No], they should explain the special circumstances that require a deviation from the Code of Ethics.
   - The authors should make sure to preserve anonymity (e.g., if there is a special consideration due to laws or regulations in their jurisdiction).

10. **Broader impacts**

    Answer: [Yes]

    Justification: The Impact Statement discusses both positive impacts, such as improving the efficiency and interpretability of LLM post-training, and potential negative impacts, such as reducing the cost of improving harmful models.

    - The answer [N/A] means that there is no societal impact of the work performed.
    - If the authors answer [N/A] or [No], they should explain why their work has no societal impact or why the paper does not address societal impact.
    - Examples of negative societal impacts include potential malicious or unintended uses (e.g., disinformation, generating fake profiles, surveillance), fairness considerations (e.g., deployment of technologies that could make decisions that unfairly impact specific groups), privacy considerations, and security considerations.
    - The conference expects that many papers will be foundational research and not tied to particular applications, let alone deployments. However, if there is a direct path to any negative applications, the authors should point it out. For example, it is legitimate to point out that an improvement in the quality of generative models could be used to generate Deepfakes for disinformation. On the other hand, it is not needed to point out that a generic algorithm for optimizing neural networks could enable people to train models that generate Deepfakes faster.
    - The authors should consider possible harms that could arise when the technology is being used as intended and functioning correctly, harms that could arise when the technology is being used as intended but gives incorrect results, and harms following from (intentional or unintentional) misuse of the technology.
    - If there are negative societal impacts, the authors could also discuss possible mitigation strategies (e.g., gated release of models, providing defenses in addition to attacks, mechanisms for monitoring misuse, mechanisms to monitor how a system learns from feedback over time, improving the efficiency and accessibility of ML).

11. **Safeguards**

    Answer: [N/A]

    Justification: The paper does not release new pretrained language models or high-risk datasets. The proposed method is an acceleration framework for OPD.

    - The answer [N/A] means that the paper poses no such risks.
    - Released models that have a high risk for misuse or dual-use should be released with necessary safeguards to allow for controlled use of the model, for example by requiring that users adhere to usage guidelines or restrictions to access the model or implementing safety filters.
    - Datasets that have been scraped from the Internet could pose safety risks. The authors should describe how they avoided releasing unsafe images.
    - We recognize that providing effective safeguards is challenging, and many papers do not require this, but we encourage authors to take this into account and make a best faith effort.

12. **Licenses for existing assets**

    Answer: [Yes]

    Justification: The paper cites the existing datasets, models, and baselines used in the experiments. We follow their intended research usage.

    - The answer [N/A] means that the paper does not use existing assets.
    - The authors should cite the original paper that produced the code package or dataset.
    - The authors should state which version of the asset is used and, if possible, include a URL.
    - The name of the license (e.g., CC-BY 4.0) should be included for each asset.
    - For scraped data from a particular source (e.g., website), the copyright and terms of service of that source should be provided.
    - If assets are released, the license, copyright information, and terms of use in the package should be provided. For popular datasets, `paperswithcode.com/datasets` has curated licenses for some datasets. Their licensing guide can help determine the license of a dataset.
    - For existing datasets that are re-packaged, both the original license and the license of the derived asset (if it has changed) should be provided.
    - If this information is not available online, the authors are encouraged to reach out to the asset's creators.

13. **New assets**

    Answer: [N/A]

    Justification: The paper does not introduce or release new datasets, pretrained models, or other standalone assets.

    Guidelines:

    - The answer [N/A] means that the paper does not release new assets.
    - Researchers should communicate the details of the dataset/code/model as part of their submissions via structured templates. This includes details about training, license, limitations, etc.
    - The paper should discuss whether and how consent was obtained from people whose asset is used.
    - At submission time, remember to anonymize your assets (if applicable). You can either create an anonymized URL or include an anonymized zip file.

14. **Crowdsourcing and research with human subjects**

    Answer: [N/A]

    Justification: The paper does not involve crowdsourcing experiments or research with human subjects.

    Guidelines:

- The answer [N/A] means that the paper does not involve crowdsourcing nor research with human subjects.
- Including this information in the supplemental material is fine, but if the main contribution of the paper involves human subjects, then as much detail as possible should be included in the main paper.
- According to the NeurIPS Code of Ethics, workers involved in data collection, curation, or other labor should be paid at least the minimum wage in the country of the data collector.

15. **Institutional review board (IRB) approvals or equivalent for research with human subjects**

    Answer: [N/A]

    Justification: The paper does not involve human subjects research.

    Guidelines:

    - The answer [N/A] means that the paper does not involve crowdsourcing nor research with human subjects.
    - Depending on the country in which research is conducted, IRB approval (or equivalent) may be required for any human subjects research. If you obtained IRB approval, you should clearly state this in the paper.
    - We recognize that the procedures for this may vary significantly between institutions and locations, and we expect authors to adhere to the NeurIPS Code of Ethics and the guidelines for their institution.
    - For initial submissions, do not include any information that would break anonymity (if applicable), such as the institution conducting the review.

16. **Declaration of LLM usage**

    Answer: [N/A]

    Justification: LLMs are the subject of study and evaluation in this work, but they are not used as a non-standard component for developing the core methodology beyond the described OPD and EffOPD training framework.

    Guidelines:

    - The answer [N/A] means that the core method development in this research does not involve LLMs as any important, original, or non-standard components.
    - Please refer to our LLM policy in the NeurIPS handbook for what should or should not be described.